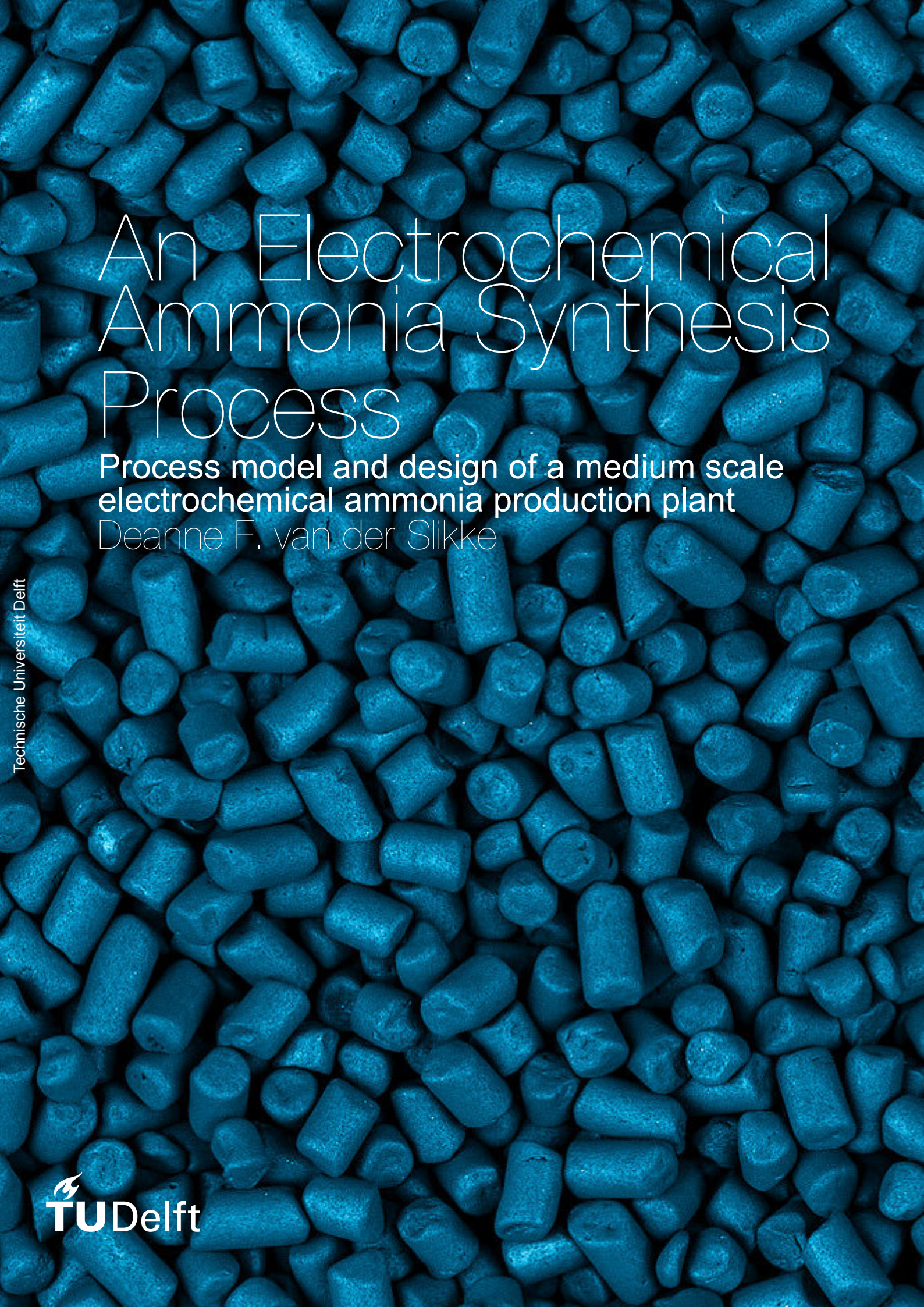

An Electrochemical Ammonia Synthesis Process

Process model and design of a medium scale electrochemical ammonia production plant

Deanne F. van der Slikke

Technische Universiteit Delft

TU Delft

An Electrochemical Ammonia Synthesis Process

Process model and design of a medium scale electrochemical ammonia production plant

by

Deanne F. van der Slikke

to obtain the degree of Master of Science
at the Delft University of Technology,
to be defended publicly on Friday August 27, 2021 at 10:00.

Student number:	4382110	
Project duration:	December 1, 2020 – August 27, 2021	
Thesis committee:	Prof.dr.ir. W. de Jong,	TU Delft
	Dr. R. Kortlever,	TU Delft, supervisor
	Dr.ir. M.d.M. Pérez-Fortes,	TU Delft
	Ir. B. Izelaar,	TU Delft, supervisor

An electronic version of this thesis is available at https://repository.tudelft.nl/.

Cover image from https://www.deltaadsorbents.com/carbon-molecular-sieve-cms220-nitrogen-generation/.

TU Delft

Preface

This master thesis is the product of all my accomplishments of the past nine months. To me, however, it also represents the knowledge I have gained, the skills I have attained and the goals I have achieved during my entire education at the Delft University of Technology. With great pleasure, I look back at a time where I met so many interesting and fun people, and where I also got to know myself. With great interest and enthusiasm I worked on this thesis, hopefully allowing for a more sustainable ammonia production technology and therefore a more sustainable future. And also, with great fulfilment, I can now close this chapter in my life and take the next step in my career.

I would like to thank my supervisors Ruud Kortlever and Boaz Izelaar for always being available for questions or brainstorm sessions, for being critical on my work and for helping me through the entire process. A special thanks to my parents and sister for always supporting me and allowing me to pursue my dreams. Thanks to my fellow students, and especially my fellow graduating friends, for accompanying me during these eccentric times and for giving me advice whenever I got tangled up in my thesis. Lastly, I would like to thank my friends for always being there for me and for helping me unstring whenever I needed it.

Deanne F. van der Slikke
Delft, August 2021

Summary

One of the greatest concerns of this century is climate change due to rising greenhouse gas emissions. The ammonia industry is responsible for 1.4% of the global CO_2 emissions, thereby having a negative climate impact. However, ammonia is an essential ingredient in nitrogen fertilisers and is also considered as a potential energy carrier. Ammonia is currently produced in the energy intensive Haber-Bosch process, where natural gas, coal or oil are used as the hydrogen and energy source. For these reasons, it is necessary to investigate more sustainable alternatives. One of the alternatives is electrochemical ammonia synthesis, where ammonia is formed out of nitrogen and water, and renewable energy sources fuel the process.

The goal of this thesis is to give insight into the required performance metrics of the electrolyser and its production process in order for this technology to become technologically feasible and competitive with a Haber-Bosch process. This is done by investigating different options for the pre-treatment, electrochemical ammonia synthesis and separation steps, and comparing their energy requirements. The final product of this thesis is a process design for an electrochemical ammonia synthesis plant with a production capacity of 1,500 tonnes per day. Cryogenic distillation and pressure swing adsorption are researched and modeled as nitrogen generators. An adsorption column for the pressure swing adsorption unit is modeled in Matlab, while Aspen is used for modeling of the distillation column. Subsequently, an alkaline and a proton exchange membrane electrolyser are considered as ammonia synthesisers. The electrochemical cells are modeled as black boxes, operating at 353 K and 1 bar and 30 bar respectively. Next, a distillation column and a flash drum are modeled in Aspen as ammonia separators. Finally, four different process diagrams are created, two that are based on an alkaline electrolyser and two based on a proton exchange membrane electrolyser. Their overall energy consumptions are analysed and for both types of electrolysers the most optimal route for ammonia production is found.

The results of this thesis point out that cryogenic distillation is preferred over adsorption for the generation of nitrogen, with an energy consumption of 0.56 $kWh \cdot kg_{N_2}^{-1}$ for compression, cooling and distillation. Adsorption can be competitive with cryogenic distillation when the nitrogen recovery rate is increased, or at lower production capacities. In a reasonable case for future electrolysers, operating at a cell voltage of 1.77 V and a Faradaic efficiency of 100%, the energy consumption for an alkaline electrolyser amounts to 12.00 $kWh \cdot kg_{NH_3}^{-1}$ and to 11.95 $kWh \cdot kg_{NH_3}^{-1}$ for a proton exchange membrane electrolyser. A distillation column was considered as utility for the separation of ammonia from the KOH solute product stream from an alkaline electrolyser. For the cathodic product stream from a proton exchange membrane electrolyser, containing only ammonia, hydrogen and nitrogen, flash separation was determined to be the best separation technology. For both separation options, it was found that an ammonia concentration of at least 10 mol% in the cell's product stream is required for an efficient separation. Ultimately, with electrolysers operating at 1.77 V and a Faradaic efficiency of 70%, the total energy consumption of an alkaline based process is equal to 17.30 $kWh \cdot kg_{NH_3}^{-1}$ and 15.45 $kWh \cdot kg_{NH_3}^{-1}$ for a proton exchange membrane based process, with overall energy efficiencies of 30% and 33% respectively. Based on the energy consumption of their respective pre-treatment and separation steps, a proton exchange membrane electrolyser is favoured over an alkaline electrolyser. In order for an alkaline based process to be advantageous, its electrochemical cell should consume at least 1.80 $kWh \cdot kg_{NH_3}^{-1}$ less than a proton exchange membrane electrolyser. Finally, currently it is not possible for AEL or PEMEL based ammonia synthesis processes to be competitive with the Haber-Bosch production process in terms of energy consumption. However, with Faradaic efficiencies of 100% and minimal overpotentials, a PEMEL based process does come close to reaching this objective.

List of Figures

List of Tables

Contents

Nomenclature

Abbreviation	Name
AEL	Alkaline Electrolyser
AEM	Anion Exchange Membrane
AEMEL	Anion Exchange Membrane Electrolyser
ASU	Air Separation Unit
CMS	Carbon Molecular Sieves
LHV	Lower Heating Value
PEM	Proton Exchange Membrane
PEMEL	Proton Exchange Membrane Electrolyser
PSA	Pressure Swing Adsorption
SMR	Steam Methane Reforming
SOEL	Solid Oxide Electrolyser
TDS	Total Dissolved Solids
TRL	Technology Readiness Level
WGS	Water-Gas Shift
WGSR	Water-Gas Shift Reaction
ZIF	Zeolitic Imidazolate Frameworks

Chemical formula	Name
CH_4	Methane
CO	Carbon monoxide
CO_2	Carbon dioxide
H^+	Hydrogen ion (proton)
H_2	Hydrogen
H_2O	Water
KOH	Potassium hydroxide
NH_3	Ammonia
O^{2-}	Oxide
O_2	Oxygen
OH^-	Hydroxide

Symbol	Definition	Unit
η_{Ω}	Ohmic overpotential (electrolyte)	V
η_{act}	Activation overpotential	V
η_{conc}	Concentration overpotential	V
η_{mem}	Ohmic overpotential (membrane)	V
ϵ	Adsorption bed voidage	-
μ	Dynamic viscosity	$Pa \cdot s$
a_{ox}	Activity oxidised species	-
a_{red}	Activity reduced species	-
A_c	Adsorption bed cross sectional area	m^2
C_i	Concentration of component i	$mol \cdot m^{-3}$
D_L	Axial dispersion coefficient	$m^2 \cdot s^{-1}$
D_p	CMS particle diameter	m
E^0	Stardard equilibrium potential half-reaction	V
E_{H-B}	Energy consumption Haber-Bosch process	$J \cdot kg_{NH_3}^{-1}$
E_{cell}	Overall cell voltage	V
E_{cell}^0	Standard equilibrium cell potential	V
E_{el}	Electrical energy consumption electrolyser	$J \cdot kg_{NH_3}^{-1}$
E_{eq}	Equilibrium potential	V
ΔE_{eq}	Equilibrium cell potential difference	V
E_{p-t}	Energy consumption pre-treatment step	$J \cdot kg_{NH_3}^{-1}$
E_{sep}	Energy consumption separation step	$J \cdot kg_{NH_3}^{-1}$
E_{th}	Thermoneutral potential	V
F	Faraday constant = 96485	$C \cdot mol^{-1}$
FE	Faradaic efficiency	%
ΔG^0	Gibbs free energy of formation	$J \cdot mol^{-1}$
H	Enthalpy	$J \cdot mol^{-1}$
I	Applied current	A
n	Electron transfer number	-
m	Mass flow rate	$kg \cdot s^{-1}$
M	Molarity	$mol \cdot L^{-1}$
M_i	Molar mass of component i	$g \cdot mol^{-1}$
p	Pressure	bar
P_{cell}	Power consumption cell	W
q_i	Adsorbed concentration of component i	$mol \cdot m^{-3}$
q_i^*	Equilibrium adsorption concentration of component i	$mol \cdot m^{-3}$
R	Universal gas constant = 8.314	$J \cdot K^{-1} \cdot mol^{-1}$
r_{H_2}	Reaction rate hydrogen	$mol \cdot s^{-1}$
r_{NH_3}	Reaction rate ammonia	$mol \cdot s^{-1}$
t	Time	s
T	Temperature	K
v	Gas flow velocity	$m \cdot s^{-1}$
V	Volumetric flow rate	$m^3 \cdot s^{-1}$
x_i	Mole fraction of component i	-
z	Length along the adsorption column	m

1 Introduction

1.1. Motivation

The rapid changes in the global climate have become a prevailing concern of mankind. Climate change includes changes in temperature, precipitation and a rise in sea levels, that consequently lead to extreme droughts, floods, storms and so on [87]. These prevailing concerns are reflected in the Paris Agreement, where goals are set and obligations are imposed to its participating countries to keep this change minimised. The most important and well-known goal of the Paris Agreement is to keep the global average temperature to well below 2 ^{o}C above pre-industrial levels and to pursue efforts to limit this increase to 1.5 ^{o}C [83].

The steady rise in atmospheric carbon dioxide concentration over the past years has led to the acceleration of global warming and climate change [86]. Therefore, it is essential to limit carbon dioxide emissions. This requires either a significant drop in energy use or a change in how we harvest, produce and use energy. Transportation, electricity production and industry are the three largest sources of carbon dioxide emissions [84]. Numerous innovations are currently researched and implemented to reduce carbon dioxide emissions in various fields. One of the industries in which a significant amount of reduction in emissions is possible is the ammonia industry. At room temperature and pressure, ammonia is a gas, but it can be liquefied by increasing the pressure to around 10 bar or by cooling it to around 240 K [49]. It is the fundamental ingredient in nitrogen fertilisers and, due to its easy liquefaction, lower heating value of 18.6 MJ $\cdot$ kg^{-1} [73] and high hydrogen content, it is considered as a potential energy carrier [43]. However, ammonia is currently produced in the energy intensive Haber-Bosch process, which is responsible for 1.4% of the global carbon dioxide emissions [82]. A less energy intensive and less carbon dioxide emitting alternative for the production of ammonia is thus necessary to reach the goals stated in the Paris Agreement.

One of the emerging technologies for ammonia synthesis is via an electrochemical route. In electrochemical ammonia synthesis, ammonia is produced directly from water and nitrogen and is driven by an electrochemical potential. This technology requires an electrical current, optimally derived from renewable energy sources, nitrogen, obtained from atmospheric air, and water as a hydrogen source instead of fossil based resources, allowing a more sustainable production of ammonia. Current research is focused on finding appropriate ion conductive materials and catalysts for electrochemical ammonia synthesis [5, 28]. However, little research is done on the larger scale implications of this process. The current work is therefore a process based analysis of electrochemical ammonia synthesis and aims to give insight into the required performance metrics of the electrolyser in order for this technology to become technologically feasible and competitive.

1.2. The need for ammonia

The global annual demand for ammonia (NH_3) was estimated to be 170 million tonnes in 2020, with a growth of 1.5% per year since 2015 [22]. This large demand for ammonia and its growth rate are caused largely by its use in the fertiliser industry. Ammonia is used in fertilisers since nitrogen, in the form of ammonia, is an essential building block for the growth of crops. Due to the growing food demand, caused by a growing world population, the demand for ammonia will keep increasing rapidly. Moreover, ammonia is used, for instance, as a refrigerant or for the manufacturing of chemicals. Besides, ammonia has the potential to act as an energy vector, where ammonia is used as an alternative energy carrier [43].

In the Haber-Bosch process, currently the most used ammonia synthesis technology, nitrogen is obtained from air, while hydrogen can be provided by a variety of sources, such as coal, oil or natural gas. The negative value for the enthalpy of formation of ammonia from nitrogen and hydrogen (Equation 1.1), indicates the exothermic behaviour of this reaction. However, due to the strong N≡N triple bond in nitrogen, reduction without a catalyst is very difficult and even with a catalyst, a considerable amount of energy is required for the activation of this molecule. Therefore, the Haber-Bosch process is carried out at temperatures of around 700 K. However, at these temperatures, the equilibrium of the reaction (Equation 1.1) shifts all the way to the left. In order to shift the equilibrium towards the right, the Haber-Bosch process is carried out at elevated pressures, favouring the production of ammonia.

$$N_2 + 3H_2 \leftrightarrow 2NH_3 \qquad \Delta H = -92 \text{ kJ} \cdot \text{mol}^{-1} \tag{1.1}$$

A less emitting and more energy efficient alternative for the Haber-Bosch process is desirable. Electrochemical ammonia synthesis, where ammonia is electrochemically derived from water and nitrogen (Equation 1.2), is suggested as an alternative technology. In electrolysis, an electric current is used to drive an otherwise non-spontaneous reaction, assisted by a catalyst. Electrochemistry is believed to be a viable technology for the carbon-free production of ammonia from renewable resources [40].

$$N_2 + 3H_2O \leftrightarrow \frac{2}{3}O_2 + 2NH_3 \qquad \Delta H = 383 \text{ kJ} \cdot \text{mol}^{-1} \tag{1.2}$$

This thesis investigates the different options for pre-treatment, electrochemical ammonia synthesis and separation steps, and aims to find the most optimal route, in terms of energy consumption, for producing ammonia. In addition, this thesis aims to formulate technological performance targets for ammonia electrolysers. First, a literature review is carried out, which serves to understand the different technologies. The literature review is concluded with the research questions. Next, the methods that are used are discussed and choices for certain technologies are justified. Hereafter, the results from the previous section are evaluated and this thesis ends with a discussion, recommendations and a conclusion.

2

Literature

2.1. Current and emerging technologies for ammonia synthesis

This section deals with the current and emerging technologies for ammonia synthesis: the Haber-Bosch process, the electrical Haber-Bosch process and electrochemical ammonia synthesis. Their technologies, characteristics, advantages and disadvantages will be discussed here.

2.1.1. Haber-Bosch process

Today, 96% of ammonia is produced through the Haber-Bosch process [78]. Fossil fuels, such as natural gas, coal and oil, provide the energy and hydrogen needed for the reactions. New ammonia plants are almost exclusively based on natural gas (methane), therefore the process based on natural gas will be elaborated in this section. The unit operations of the Haber-Bosch process will be discussed in three separate parts, namely feed pre-treatment, the core process, where hydrogen and subsequently ammonia production take place, and product separation.

The three main feeds for the process are natural gas, steam and air. The pre-treatment of natural gas mainly consists of sulphur removal and the removal of other impurities that damage the Steam Methane Reforming (SMR) catalyst. Next, steam is added to the natural gas to convert larger hydrocarbons to methane [79]. Conventionally, two SMR reactors consecutively convert methane to syngas (a mixture of mainly hydrogen and carbon monoxide). In the second steam reformer, oxygen is used, as will be shown later in this section. Later on in the process, nitrogen is needed for the formation of ammonia. Therefore, air, which is rich in both nitrogen and oxygen, is injected before the second steam reformer and little pre-treatment is needed. When a single SMR reactor is used, an additional air separation unit is required for the separation of nitrogen from air.

The core part of the process consists of two SMR reactors, a Water-Gas Shift (WGS) reactor and the Haber-Bosch reactor itself, as can be seen in Figure 2.1. In the first SMR reactor, syngas is formed in the highly endothermic reaction of methane with steam (Equation 2.1). Additional natural gas is burned to provide the necessary heat for this reaction.

$$CH_4 + H_2O \rightarrow CO + 3H_2 \qquad \Delta H = 206\ \text{kJ} \cdot \text{mol}^{-1} \tag{2.1}$$

In order to increase the hydrogen yield, unconverted methane reacts in a second SMR reactor. In this case, air is injected as an oxygen source and as a nitrogen source for the ammonia synthesis downstream. The second SMR reactor is autothermal because the feed stream is heated by the first SMR reactor and the reaction is exothermic (Equation 2.2).

$$2CH_4 + O_2 \rightarrow 2CO + 4H_2 \qquad \Delta H = -71\ \text{kJ} \cdot \text{mol}^{-1} \tag{2.2}$$

The next step is the WGS reaction (WGSR). Additional steam is added and carbon monoxide is converted to carbon dioxide and more hydrogen (Equation 2.3).

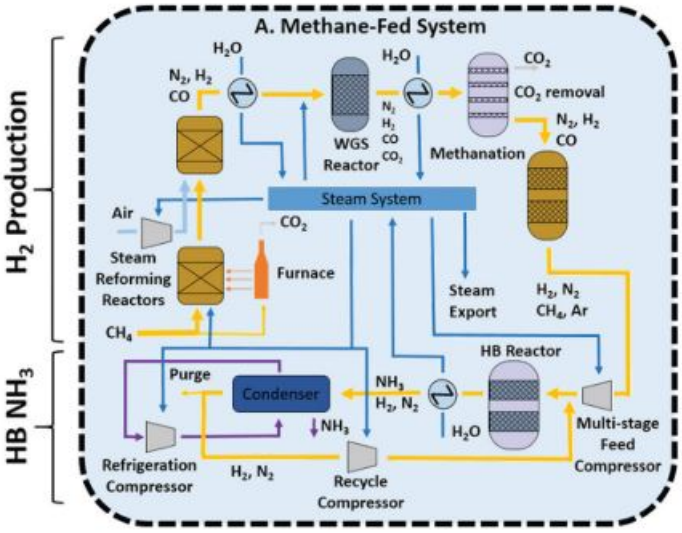

Figure 2.1: Schematic diagram of the conventional Haber-Bosch process. Yellow lines: process gas, dark blue lines: water/steam, light blue lines: air, purple lines: ammonia. Reprinted from reference [78].

$$CO + H_2O \rightarrow CO_2 + H_2 \qquad \Delta H = -41\ \text{kJ} \cdot \text{mol}^{-1} \tag{2.3}$$

Subsequently, carbon dioxide is removed and the gas mixture is compressed and fed to the Haber-Bosch reactor, where nitrogen and hydrogen are converted into ammonia (Equation 1.1). The Haber-Bosch reactor typically operates at 15-25 MPa and 675-725 K [78]. These high temperatures have an adverse effect on the formation of ammonia. Therefore the reaction typically takes place at elevated pressures, thereby favouring the formation of ammonia and increasing the single-pass conversion rates. However, the conversion rates are still low and a recycle is needed to increase the ammonia production rate.

In conventional Haber-Bosch processes, ammonia is separated by condensation at temperatures of around 248 K [8]. Unreacted hydrogen and nitrogen are compressed, reheated and recycled into the ammonia synthesis loop.

Stoichiometrically, the Haber-Bosch process, including SMR and WGSR, emits 1.07 $kg_{CO_2} \cdot kg_{NH_3}^{-1}$ (calculation can be found in Appendix A). The emissions are higher in reality and have been estimated to be 1.5 $kg_{CO_2} \cdot kg_{NH_3}^{-1}$ [68]. Although this number has decreased since the introduction of this technology and integrated carbon capture technologies are being developed [34], a process that is independent of fossil fuels is highly desirable. Moreover, the Haber-Bosch process is an energy intensive process, that requires an energy input of 7.7 - 8.8 $kWh \cdot kg_{NH_3}^{-1}$ [20]. The lower heating value (LHV) of a fuel is the total amount of heat that is liberated during the combustion of a fuel minus the latent heat of vaporisation. In other words, the LHV is the amount of heat that is available when the fuel is burned in an engine. With a LHV for ammonia of 5.17 $kWh \cdot kg_{NH_3}^{-1}$ [33], this indicates an average energy efficiency of 62.67%.

2.1.2. Electrical Haber-Bosch process

Hydrogen, needed for ammonia synthesis, can be produced through different routes. In the classical Haber-Bosch process, hydrogen is obtained from natural gas. However, hydrogen can also be obtained, for instance, from conversion of biomass or through water electrolysis [58, 98]. The electrical Haber-Bosch process is based on the latter. Electricity, optimally derived from a renewable energy source, is used to split water into oxygen and hydrogen. Hereafter, nitrogen is reacted with the obtained hydrogen in a similar Haber-Bosch process as described before.

Using electricity from renewable energy sources decreases the carbon footprint of the ammonia

production process (compared to a Haber-Bosch process with SMR). A wind energy powered electrical Haber-Bosch process is estimated to emit 0.12 - 0.53 $kg_{CO_2} \cdot kg_{NH_3}^{-1}$, where the carbon intensity largely depends on the size of the wind turbine [78]. Also, energy losses are reduced due to a decrease in compression losses and higher achieved product purity. This reduces the need for purge and allows the possibility of powering the compressors more efficiently [78]. Although less heat integration is possible, energy losses are decreased by 1.17 kWh [78], resulting in a required energy input of 6.83 $kWh \cdot kg_{NH_3}^{-1}$. However, the future of electrical Haber-Bosch processes will largely depend on the electrolyser efficiency [78]. Moreover, installation and operation costs need to be reduced, while reliability, durability and safety need to be increased.

If a fully sustainable process is desired, ammonia can only be produced when there is a surplus of renewable energy. However, most renewable energy sources are non-dispatchable and therefore highly intermittent. This requires either flexibility in ammonia production, with high ramp rates, or hydrogen or battery storage to ensure continuous ammonia production. The former is hard to realise due to the inability of high pressure processes with extensive heat integration to operate outside steady-state, while the latter leads to an increase in capital costs and asks for additional advancements in the considered technology. In fact, battery storage is currently too expensive, thus hydrogen storage will be needed to ensure continuous ammonia production during periods of renewable energy shortages [49].

2.1.3. Electrochemical ammonia synthesis

The last ammonia synthesis route that will be described in this section is inspired by the natural process where nitrogen from the atmosphere is reduced to ammonia under the presence of nitrogenase enzymes. In electrochemical ammonia synthesis, a catalyst stimulates the reduction of nitrogen to ammonia with the electrochemical potential as thermodynamic driving force. In contrast to the Haber-Bosch process, electrochemical ammonia synthesis can take place at near ambient temperatures and pressures, possibly favouring the production of ammonia [88].

The amount of energy required for electrochemical ammonia production depends firstly on the energy required in the form of two half-reaction potentials. These half-reactions depend on the type of electrolytic cell. Different options for these cells will be discussed in section 2.3. The Gibbs free energy of formation (ΔG^0) for the reduction of nitrogen with water is equal to 5.54 $kWh \cdot kg_{NH3}^{-1}$ (see Appendix B). This value indicates the minimum amount of energy needed for the electrochemical formation of ammonia. The overall reaction for the electrochemical nitrogen reduction into ammonia is as follows:

$$N_2 + 3H_2O \rightarrow \frac{3}{2}O_2 + 2NH_3 \tag{2.4}$$

Three moles of electrons are transported for the formation of one mole of ammonia (n = 3), leading to a standard equilibrium cell potential $E^0_{cell} = -1.17$ V (Equation 2.5).

$$E^0_{cell} = -\frac{\Delta G^0}{n \cdot F} = -1.17 \text{ V} \tag{2.5}$$

Where F is Faraday's constant. The standard equilibrium cell potential, also called the reversible cell voltage, is the difference between the standard equilibrium potentials of the half-reactions (E^0). The overall cell voltage is a summation of the reversible cell voltage and several terms for irreversible voltages, also called overpotentials [17]. The first correction gives an equilibrium potential for each of the half reactions and takes into account the influence of the temperature and activity of the oxidised and reduced species, a_{ox} and a_{red} respectively, as described by the Nernst equation:

$$E_{eq} = E^0 + \frac{RT}{n \cdot F} \ln\left(\frac{a_{ox}}{a_{red}}\right) \tag{2.6}$$

The difference between the equilibrium potentials of the half-reactions gives the equilibrium cell potential difference, ΔE_{eq}. The overall cell voltage (E_{cell}), however, is a summation of the equilibrium cell potential difference, an activation overpotential (η_{act}), concentration overpotential (η_{conc}), and a

resistance due to the electrolyte (η_{Ω}) and membrane (η_{mem}).

The difference between the equilibrium potentials of the half-reactions gives the equilibrium cell potential difference, ΔE_{eq}. The overall cell voltage (E_{cell}), however, is a summation of the equilibrium cell potential difference, an activation overpotential (η_{act}), concentration overpotential (η_{conc}), and a resistance due to the electrolyte (η_{Ω}) and membrane (η_{mem}).

$$E_{cell} = \Delta E_{eq} + \eta_{act} + \eta_{conc} + \eta_{\Omega} + \eta_{mem} \tag{2.7}$$

Factors influencing each of these terms are summarised bellow:

- The activation overpotential is related to the energetic barrier that needs to be overcome to start electron transfer and thus the reaction. η_{act} is closely related to the catalyst.
- The concentration overpotential is related to a boundary layer on the electrode surface, for instance when a reactant is rapidly consumed at the electrode, resulting in concentration differences.
- The overpotential associated with the electrolyte is influenced by the electrolyte conductivity and volume, and by the current density.
- The overpotential associated with the membrane is influenced by the membrane's resistance, conductivity and thickness, and by the current density.

The power consumed by a cell (P_{cell}) is calculated as follows:

$$P_{cell} = E_{cell} \cdot I \tag{2.8}$$

where I is the applied current.

Subsequently, the electrical energy consumption for the production of one mole ammonia (E_{el}) is found by division of the consumed power by the ammonia production rate r_{NH_3} (in mol $\cdot$ s^{-1}):

$$E_{el} = \frac{P_{cell}}{r_{NH_3}} \tag{2.9}$$

Finally, additional energy needs to be provided for feed pre-treatment, compression, heating and product separation. Since electrochemical ammonia synthesis is still at a low technology readiness level (TRL), no real-life data is available for its energy consumption. However, a full techno-economic analysis has estimated an energy consumption of around 17 kWh $\cdot$ $kg_{NH_3}^{-1}$ [29]. One of the challenges is the achievement of sufficient energy efficiency and ammonia production rate at the same time, which largely depends on finding the right catalyst [49]. Another subject that needs more elaboration are the technological performance targets for electrochemical ammonia synthesis. Currently, most articles refer to the ARPA-e REFUEL guidelines [29, 30, 49]. However, these guidelines are set by a Unites States government agency in 2016, are not well justified and are focused on ammonia as a fuel. Therefore, this work aims to reformulate these technological targets from a process point of view.

2.2. Pre-treatment technologies

Water and nitrogen are the main feeds for electrochemical ammonia synthesis. These components are not readily available, or at least not in large quantities. Therefore, nitrogen and water need to be obtained from their resources, air and some kind of water resource respectively, and purified up to a desired purity that differs per electrochemical technology. Nitrogen can be obtained from air through an Air Separation Unit (ASU), while water needs to be purified for use in an electrolyser. Different technologies and requirements for pre-treatment for ammonia production will be described in this section.

2.2.1. Air separation

Air is used as a nitrogen source for the synthesis of ammonia. However, atmospheric air is made up of multiple components, such as nitrogen, oxygen and argon. The components present in dry air with their respective mol% are given in Table 2.1. For example, it is necessary to remove oxygen from the feed gas, since it will otherwise react with protons in the electrochemical cell to form H_2O and hence reduce the Faradaic efficiency [40]. This section describes different air separation methods that are suited to provide nitrogen for electrochemical ammonia synthesis.

Table 2.1: Composition of dry air [85].

Component	Concentration (mol%)	Boiling point (K)
Nitrogen, N_2	78.08	77.35
Oxygen, O_2	20.95	90.15
Argon, Ar	0.93	87.25
Helium, He	0.005	4.25
Neon, Ne	0.0018	27.05
Carbon dioxide, CO_2 [59]	0.000415	194.69
Krypton, Kr	0.00011	119.95
Xenon, Xe	0.000009	165.15

Cryogenic air separation

Cryogenic air separation is the oldest method for the separation of the different components of air, invented by Carl Linde in 1895 [12]. Nowadays, this method is still used on large scales for the separation of air and also for obtaining nitrogen for the Haber-Bosch process. Cryogenic air separation relies on the different condensation temperatures of the different components of which air is constituted. The critical temperature and pressure of air lie at T_{crit} = 132.5 K and p_{crit} = 37.7 bar, meaning that air can only be liquefied below temperatures of 132.5 K. This leads to a very energy intensive process for the cooling of air. Cryogenic distillation units exist that separate all different components present in air. However, only nitrogen is needed for the production of ammonia. Figure 2.2 shows a schematic diagram of a simplified cryogenic air separation process where each unit has its own function:

- Ambient air is filtered to remove any dust particles that may be present in atmospheric air. Hereafter, the air stream is compressed to a pressure of around 6 bar.
- In a direct contact cooler, process air is cooled through the evaporation of water.
- Carbon dioxide, water vapour and hydrocarbon are removed in one of the two (or more) molecular sieve units, that are utilised alternately in order to allow for regeneration of the sieves.
- Purified process air is cooled to liquefaction temperature of 101 K at 6 bar.
- Purified and cooled process air enters the distillation column at an intermediate stage. In the distillation column, a nitrogen enriched stream, which has a lower vapour pressure than most other components of air, will leave at the top of the distillation column, while an oxygen enriched stream, leaves at the bottom of the distillation column.
- A condenser and reboiler are commonly added to distillation columns to provide respectively a vapour and liquid flow to feed the cascade.

Cryogenic air separation is known to be very capital and energy intensive. Cryogenic ASUs are not designed for operation outside steady-state, due to their comprehensive heat integration [7, 36]. However, cryogenic ASUs are widely used due to their large production capacities with high nitrogen purities. Linde's GAN cryogenic distillation units, for instance, are able to produce 99.9999 mol% purity nitrogen at production rates of up to 2,500 $Nm^3 \cdot h^{-1}$ [46].

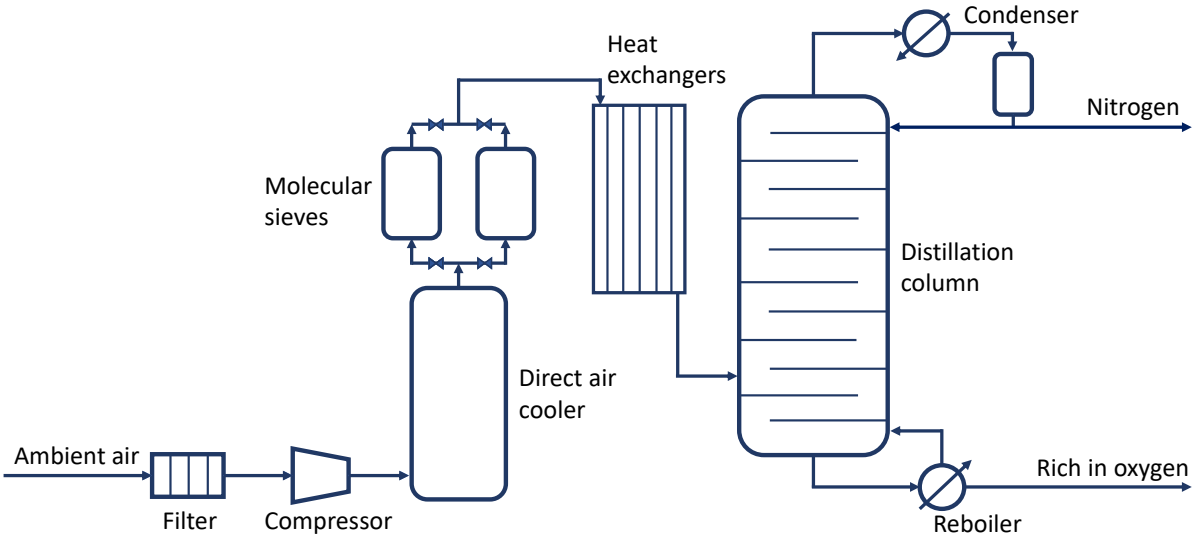

Figure 2.2: Schematic diagram of a simplified cryogenic air separation process

Pressure Swing Adsorption

For long, other methods than cryogenic methods were not well suited for air separation due to their small capacities and low product purities. However, other methods, such as Pressure Swing Adsorption (PSA), are becoming more and more attractive with improvements in volume, product purities and production flexibility [80]. PSA methods are driven by the concept of adsorption, where generally oxygen is adsorbed onto an adsorbent bed, while nitrogen is able to pass and leave the vessel. Figure 2.3 shows a schematic diagram of a simplified PSA process, where nitrogen is obtained from air through the following steps:

- Ambient air is pre-filtered of dust and compressed to increase the air flow.
- Air enters one of the adsorbers where carbon dioxide and residual moisture are adsorbed at the entrance of the vessel. The vessels are packed with carbon molecular sieves and, when in use for nitrogen separation, the vessel is pressurised, thereby selectively adsorbing oxygen onto the surface of the adsorbent, while nitrogen is able to pass.
- Gaseous nitrogen can be stored in a buffer tank if nitrogen production and consumption are not exactly matched.
- When the carbon molecular sieves of one vessel are saturated with oxygen, and thus its performance has declined, the valves are switched and air starts to flow through the other vessel. The saturated vessel is depressurised, thereby releasing the adhered oxygen molecules while air flows past the sieves. An oxygen enriched purge stream leaves the vessel and the vessel can be used again for air separation. The use of two (or more) vessels allows for continuous nitrogen production.

One of the advantages of PSA for nitrogen generation is its process simplicity, especially compared to cryogenic distillation of air, thereby reducing capital cost. Due to its use of pressure instead of temperature for the separation of nitrogen from air, this process is able to use efficient electrical compressors, making this method better compatible with renewable energy. Moreover, with this technique, sufficient nitrogen flow rates with appropriate purity can be achieved. As an example, Air Products' PRISM Nitrogen Generation System can deliver nitrogen with a purity of up to 99.9995 mol% at 2,600 $Nm^3 \cdot h^{-1}$ [3]. Although PSAs operate most economically at full capacity, these processes are very flexible, since they can start up and power down within minutes [32, 80].

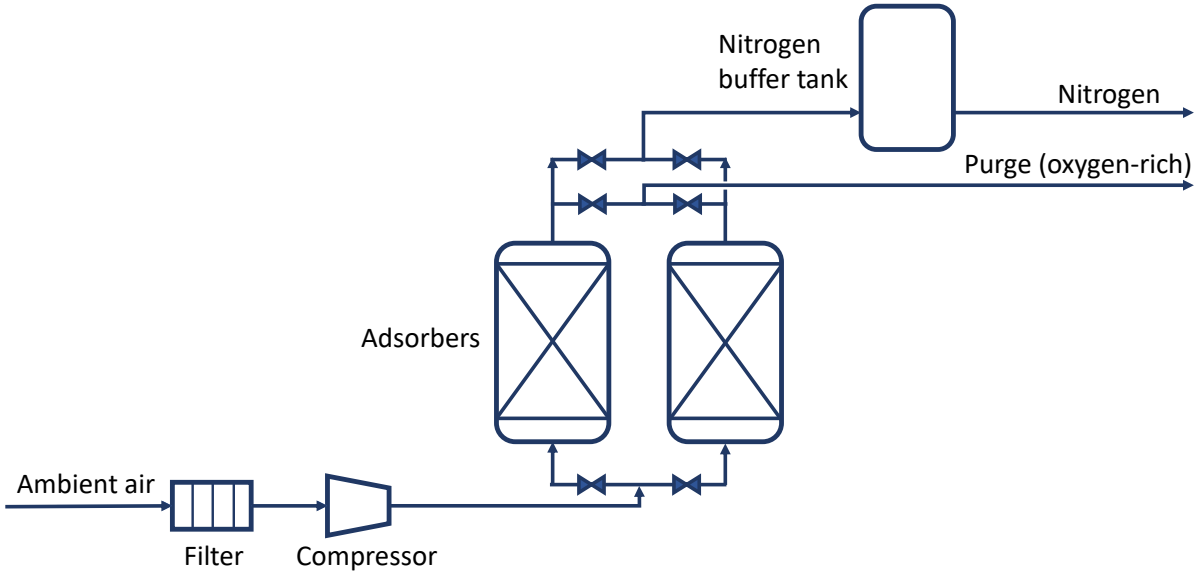

Figure 2.3: Schematic diagram of a simplified pressure swing adsorption process.

Membrane air separation

The last technology for air separation that will be discussed in this section is membrane air separation and is based on the different permeabilities of the different components of air. Permeability is a function of a molecule's ability to dissolve in, diffuse through and dissolve out of the membrane. The selectivity of a membrane is the ratio of the permeabilities of the components that need to be separated.

The process of membrane air separation is comparable to the process of a PSA system, but the adsorber is replaced by a vessel filled with either thousands of hollow fibres or spiral wound sheets, the membranes. Pre-filtered and dried air is pressurised, enters the vessel and flows through the fibres or tubes. A pressure difference causes a flow through the membrane. However, due to their specific permeability, some components are more likely to permeate the membrane, mainly due to their size [80]. Oxygen and carbon dioxide are smaller in size than nitrogen and therefore permeate the membrane more easily. A nitrogen-rich product stream will thus leave the fibres, while an oxygen-rich stream will be found on the permeate side of the membrane. Figure 2.4 shows a schematic representation of this process.

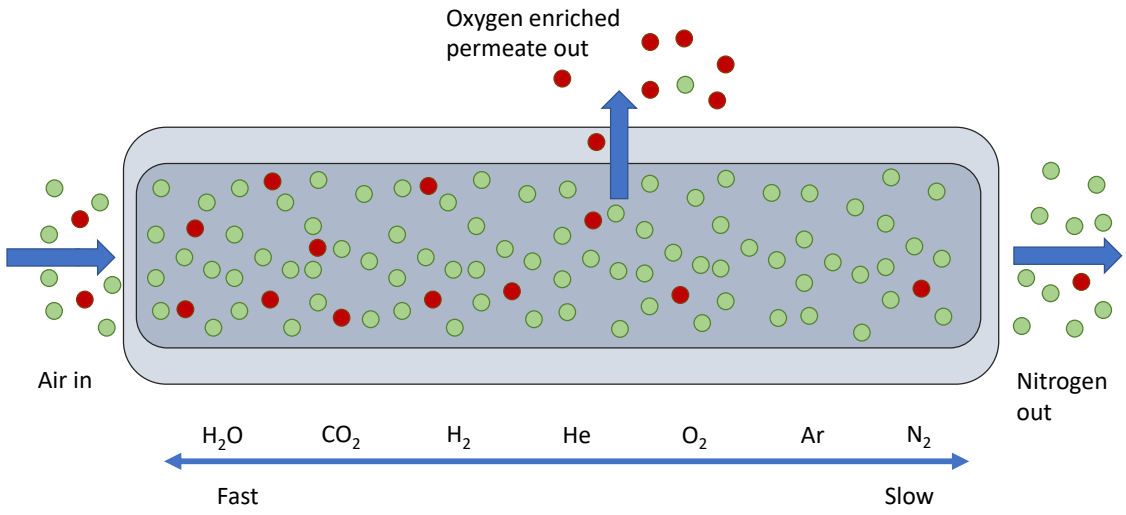

Figure 2.4: Schematic diagram of an air separation fibre, the relative permeation rates for different components are represented by the arrow. Red: oxygen molecules, green: nitrogen molecules.

Capital investment for membrane air separation systems are generally a linear function of the desired production rate, where more membranes are installed parallel with increasing demand [76]. As with PSA systems, membrane ASUs have a fast start-up time, due to their near ambient operation, and are compatible with renewable energy to run their compressors. The downside of membrane air separators is their limited product purity and smaller capacities compared to cryogenic distillation and PSA. The Membrane Nitrogen Generation systems from Air Products is able to achieve nitrogen purities of 99.9 mol% at a nitrogen flow rate of 800 $Nm^3 \cdot h^{-1}$ [2].

2.2.2. Water purification

Feed water impurities lead to by-products in the electrolytic cell and thereby reduce the Faradaic efficiency [41]. Therefore, the feed water needs pre-treatment to attain high purity levels. Generally, water is filtered and treated to remove any residual bacteria [10]. Subsequently, deionisation of water takes place to reduce the amount of particles that may hinder the desired reaction in the elecrolyser. Different electrolyser types accept different water purities. Alkaline electrolysers require a water purity of 10 ppm total dissolved solids (TDS) [57], while solid oxide electrolysers and proton exchange membrane electrolysers require process water with a maximum of 0.5 ppm TDS [56]. When the accepted water purity is achieved, the purified water may be used directly in the subsequent process or is stored in vessels for later use.

In arid regions, with fresh water scarcity, the use of fresh water for ammonia production may give rise to new problems such as competition with its use as drinking water. Consequently, seawater is regularly suggested to be used instead of fresh water [18, 49, 63]. However, seawater needs intensive pre-treatment to remove all organic and in-organic particles. Seawater can be desalinised through thermal distillation or by membrane separation, where the former involves heat and the latter pressure for separation purposes. Thermal distillation, that utilises renewable resources for heating, has low efficiencies compared to membrane separation, or more specifically, reverse osmosis [99]. Reverse osmosis mainly utilises pumps to create a pressure difference, making it therefore an adequate technology for using renewable electrical energy.

2.3. Electrolytic cells for ammonia synthesis

The actual conversion of nitrogen and water to ammonia takes place in the electrolytic cell. This section describes important individual cell components and the cell's operating variables. Moreover, different types of electrolytic cells will be discussed and each of their advantages and disadvantages are reviewed.

2.3.1. Factors influencing ammonia formation in the electrolytic cell

Ammonia formation rate, Faradaic efficiency and cell potential are three important values that characterise the performance of electrolytic cells. The first two are preferably maximised, but otherwise balanced as much as possible, while the overpotential is ideally minimised. The ammonia formation rate typically lies in the range of $10^{-13} - 10^{-8}$ $mol \cdot cm^{-2} \cdot s^{-1}$ [28], while the Faradaic efficiencies differ largely for different electrolysers. First, two important components of an electrolytic cell, the electrolyte and electrodes, will be described. Then the influence of the operating temperature is analysed. Finally, the behaviour and influence of the applied current and imposed cell potential are outlined.

Electrolyte

The electrolyte is the medium between the two electrodes. The properties of the electrolyte are of utmost importance to the performance of the electrolytic cell and become more and more concerning with increasing temperature and pressure [28]. In order to transport ions effectively, and thus minimise ohmic losses, the electrolyte must exhibit high ionic conductivity, typically in the range of 10^{-3} - 10^{-1} $S \cdot cm^{-1}$ [5, 25]. The conductivity of the electrolyte increases almost linearly with temperature, while the thickness of the electrolyte layer is inversely related to its conductivity [26]. However, a certain electrolyte layer thickness is required for mechanical stability. Moreover, solid electrolytes

must be dense to prevent crossover of product gases and have similar thermal expansion coefficients as other cell components, this is especially relevant for high temperature electrolysis [5, 28].

Electrode

The electrodes must show both electric conductivity, since the electrodes convey electrons to the surface where the reactions take place, and catalytic activity, for breaking the molecular nitrogen triple bond and, subsequently, the synthesis of ammonia [25, 28]. In order to increase the Faradaic efficiency of the system, the working electrode should prevent the delivered H^+ from forming gaseous hydrogen, i.e. it should suppress the hydrogen evolution reaction [53]. Therefore, Marnellos et al. [54] suggested palladium-based electrodes in 1998 to promote ammonia formation, while suppressing hydrogen formation. Since then numerous different catalysts have been tested, such as ruthenium, platinum and silver based catalysts, as well as conductive oxides and composite materials [4, 38, 42, 48, 93]. Moreover, the electrodes should exhibit long-term stability under the operating temperatures and current densities, and have sufficient catalytic surface area [5]. Currently, the challenge lies in finding a well suited electrode material for electrochemical ammonia synthesis [25].

Temperature

As described earlier, operating temperature influences the ionic conductivity of the electrolyte. Consequently, an increase in ionic conductivity leads to an increase in the ammonia formation rate. Experiments conducted in low temperature electrolysis (298 - 373 K), intermediate (373 - 673 K) and high temperature electrolysis (573 - 873 K) confirm this interpretation and indeed show an increase in ammonia formation with increasing temperature [13, 31, 48]. However, after a certain temperature, a decrease in ammonia formation was observed. For low temperature electrolysis (see Figure 2.5a) this phenomenon is associated to a decrease in proton conductivity due to water loss in the membrane. For high temperature electrolysis on the other hand (see Figure 2.5b), this can be attributed to the decomposition of ammonia at such high temperatures, to such an extent that the increase in ammonia formation is not able to keep up with the simultaneous decomposition of ammonia. Moreover, elevated operating temperatures lead to faster degradation of the cell and its main components and higher investment costs [28]. It should be noted that for high temperature electrolysis reasonable Faradaic efficiencies have been demonstrated, while for low temperature electrolysis Faradaic efficiencies generally do not exceed 1% (yet) [90].

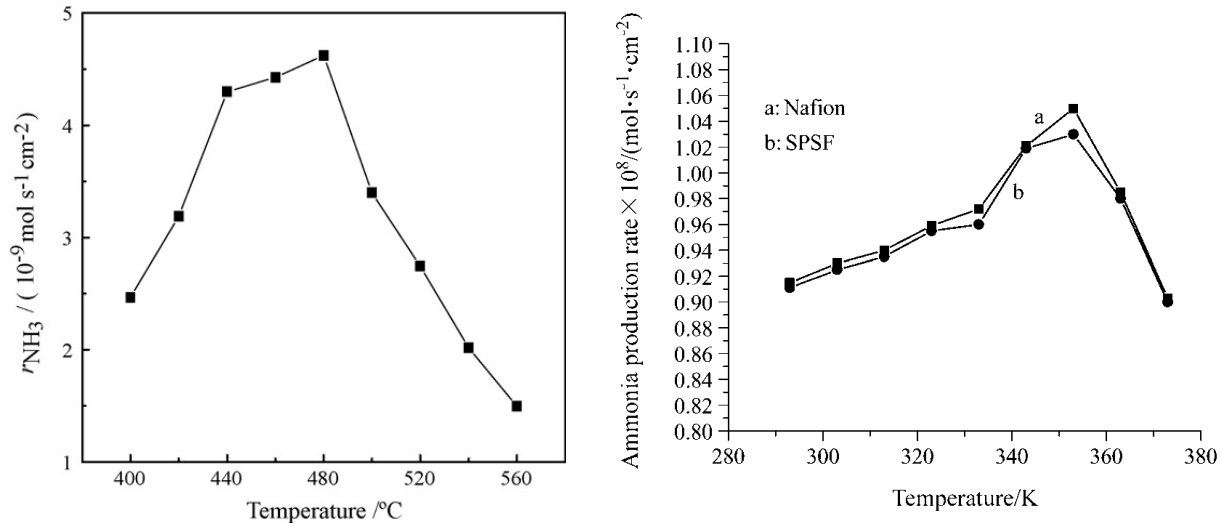

(a) For low operating temperature [48].

(b) For high operating temperature [13].

Figure 2.5: Dependence of ammonia formation rate on the operating temperature.

In summary, a balance needs to be found between the operating temperature and the ammonia production. Thereby reducing investment and operating costs and material degradation at lower temperatures, while keeping ionic conductivity and ammonia formation sufficiently high. There are limiting factors for the operating temperature for each cell type and the optimal operating temperature differs per electrolyte, membrane and catalyst.

Current

The applied current determines the rate of reaction at the electrodes. When a current is absent, no electrons will be provided and thus no ammonia can be formed at the cathode. Upon imposing a current, the rate of electron flow will increase, and thus the rate of ammonia formation will increase [5]. Wang et al. [93] investigated the ammonia formation rate as a function of the applied current and found that indeed the rate of ammonia formation increased with increasing current. However, they also found a strong decrease of ammonia formation after 0.5 mA · cm^{-2} (applied current of 1 mA at a surface area of 0.5 cm^2), as can be seen in Figure 2.6. This decrease in ammonia formation may be due to the high rate of H^+ supply, subsequently poisoning the catalyst, favouring the formation of gaseous hydrogen and thereby hindering ammonia formation [25].

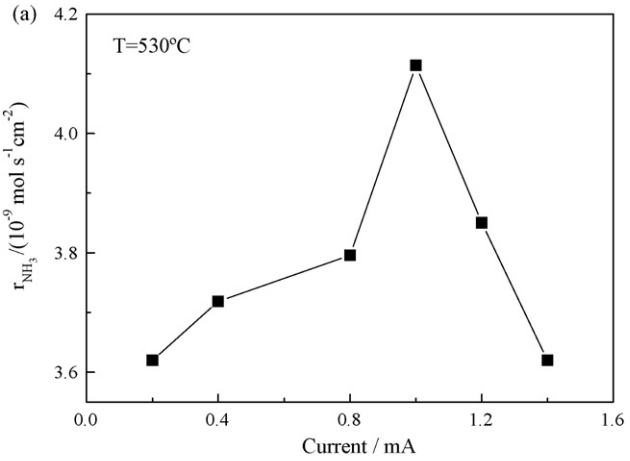

Figure 2.6: Dependence of ammonia formation rate on the applied current. The current is applied at a surface area of 0.5 cm^2 and therefore the current density is $0.5I\ mA \cdot cm^{-2}$. Reprinted from reference [93].

Faradaic efficiency is a measure to describe the amount of current that is used to produce the desired product, ammonia in this case. Faradaic efficiency changes rapidly with changing voltage, current and temperature [14, 16], and a trade-off needs to be made between these parameters. Xu et al. [97] investigated the electrochemical synthesis of ammonia from nitrogen and hydrogen with a Nafion membrane as proton conductor. The highest rate of ammonia formation was found at 350 K and 2 V and was equal to $1.13 \cdot 10^{-8}$ mol · cm^{-2} · s^{-1}, with a Faradaic efficiency of 90.4%. Faradaic efficiencies for ammonia synthesis from nitrogen and water, on the other hand, resulted in much lower Faradaic efficiencies. Lan et al. [42] obtained Faradaic efficiencies of 0.83% at 350 K, 1.2 V and an ammonia formation rate of $9.37 \cdot 10^{-10}$ mol · cm^{-2} · s^{-1}.

Cell potential

The imposed cell potential has an influence on the transport of charge between the two half-cells, and thus on the formation of ammonia. In subsection 2.1.3, it has been found that the standard equilibrium cell potential E^0_{cell} = -1.17 V. Taking into account that additional potential (overpotential) needs to be applied to overcome resistances, the overall cell potential (E_{cell}) always needs to more negative than -1.17 V.

The thermoneutral potential is the potential where not only the reaction takes place, but also the heat that is produced during the reaction is sufficient to keep a constant temperature. The thermoneutral potential (E_{th}) is given by:

$$E_{th} = -\frac{\Delta H^0}{n \cdot F} \tag{2.10}$$

With a change in enthalpy at standard equilibrium conditions (ΔH^0) of 382.55 kJ $\cdot$ mol^{-1} and an electron transfer number of n = 3 for the formation of one mole of ammonia, the thermoneutral potential $E_{th} = -1.32$ V. When the imposed cell potential is larger than the thermoneutral potential, heat will be generated.

When no cell potential is applied, no ammonia will be formed at the cathode and with increasing cell potential, the ammonia formation rate increases as well [45]. Limited research has been done on the relation between cell potential and ammonia formation rate in ammonia synthesis from nitrogen and water. However, Liu et al. [47] carried out a similar research for ammonia synthesis from nitrogen and hydrogen. For several proton-conducting ceramics, they found that the ammonia production rate increased significantly when the cell potential was increased from 0 to 0.6 V, but beyond this voltage, an increase in potential only led to a minor increase in ammonia formation. It is expected that similar results can be found for ammonia synthesis from nitrogen and water, because the electrochemistry is comparable. A study on ammonia synthesis from nitrogen and water by Chen et al. [15] indeed pointed out that ammonia formation was low and constant with cell potentials between 0 and -1.5 V. When the cell potential was changed to -2 V, the ammonia formation rate was increased to $3.6 \cdot 10^{-12}$ mol $\cdot$ cm^{-2} $\cdot$ s^{-1}. Further research should be carried out to analyse the effect of the cell potential on ammonia formation rate between -1 and -2 V in further detail.

2.3.2. Types of electrolytic cells

Electrochemical conversion of nitrogen and water to ammonia takes place in an electrolytic cell. Electrolytic cells are primarily composed of two electrodes (anode and cathode) and a conductive material separating them. This section deals with four types of electrochemical cells for ammonia synthesis: an alkaline electrolyser (AEL), a proton exchange membrane electrolyser (PEMEL), solid oxide electrolyser (SOEL) and an anion exchange membrane electrolyser (AEMEL), whose corresponding cells are depicted in Figure 2.7.

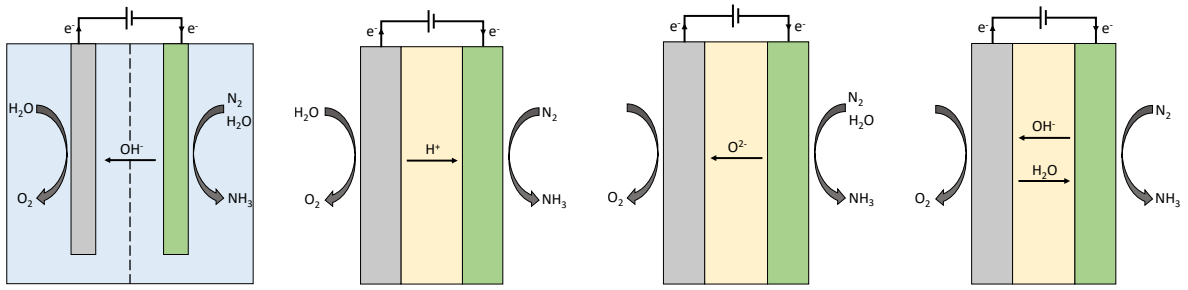

(a) AEL (b) PEMEL (c) SOEL (d) AEMEL

Figure 2.7: Schematic diagrams of four simplified electrochemical ammonia synthesis cells (blue: alkaline solution, grey: anode, green: cathode, yellow: membrane).

2.3.3. Alkaline electrolysers

AELs are characterised by two electrodes that are placed in a liquid alkaline electrolyte, typically consisting of a concentrated potassium hydroxide (KOH) or sodium hydroxide (NaOH) solution, as depicted in Figure 2.7a. A diaphragm separates the two electrodes and prevents mixing of the gaseous products, while allowing passage of hydroxide ions (OH^-). These hydroxide ions react at the anode to gaseous oxygen and water as follows:

$$6OH^- \rightarrow \frac{3}{2}O_2 + 3H_2O + 6e^- \tag{2.11}$$

Electrons are released in this oxidation reaction, driven by the applied potential. These electrons are used for the reduction half-reaction that takes place at the cathode. Here, nitrogen and water react to form ammonia and OH^-:

$$N_2 + 6H_2O + 6e^- \rightarrow 2NH_3 + 6OH^- \tag{2.12}$$

Alkaline electrolysis is a mature technology that was already commercialised for water splitting in the late 19th century [96]. Consequently, AELs are well optimised, efficient and cheap in comparison to newer technologies. However, current densities are lower in comparison to other water electrolysers and product crossover through the diaphragm can be problematic for the nitrogen reduction reaction as this might cause lower ammonia purities compared to other technologies [67]. Moreover, their load range is limited due to crossover of hydrogen to the oxygen side at low production rates, resulting in a flammable mixture. Also, cold start-up times are long (typically 2 hours) to prevent gas leakage and minimise mechanical stress due to a change in temperature [11]. Warm start-up times are reasonable (1 - 5 minutes) and AELs can be held in stand-by mode to ensure flexible operation. However, stand-by losses will have to be taken into account.

2.3.4. Proton exchange membrane electrolysers

PEMELs rely on the conduction of protons, as can be seen in Figure 2.7b. Nafion® membranes are the most popular proton conducting membranes for proton exchange membrane (PEM) electrolysis and serve as a separator between the two half-cells [28]. At the anode, water is converted to gaseous oxygen and protons (H^+):

$$3H_2O \rightarrow \frac{3}{2}O_2 + 6H^+ + 6e^- \tag{2.13}$$

The proton conductivity of the membrane allows the H^+ diffusion and migration towards the cathode where it reacts with nitrogen to ammonia:

$$N_2 + 6H^+ + 6e^- \rightarrow 2NH_3 \tag{2.14}$$

Advantages of PEMELs are their ability to operate at high current density, their compact system design and high purity products production [67]. Their ability to operate at partial load and shorter start-up rates compared to AEL, due to a more compact system and lower heat capacities, are advantageous for flexible operation [11]. However, capital investment for these electrolysers is significant due to the requirement for noble metal catalysts that are able to tolerate the acidic environment caused by the membrane [11, 23]. This corrosive acidic environment also causes the durability of these cells to be comparatively low. However, PEMELs are on their way to be commercialised and research is conducted on improving their performances.

2.3.5. Solid oxide electrolysers

SOELs are characterised by a membrane that conducts either oxides (O^{2-}) or protons (H^+) and typically operates at elevated temperatures of up to 1200 K [11, 21]. The oxidation and reduction half-reactions for proton conducting SOEL are the same as for PEMELs (Equation 2.13 and Equation 2.14), while in oxide conducting SOELs, O^{2-} ions react at the anode to gaseous oxygen and at the same time electrons are released:

$$3O^{2-} \rightarrow \frac{3}{2}O_2 + 6e^- \tag{2.15}$$

The O^{2-} ions are formed in the reduction half-reaction at the cathode, where nitrogen and water react to ammonia and O^{2-} ions:

$$N_2 + 3H_2O + 6e^- \rightarrow 2NH_3 + 3O^{2-} \tag{2.16}$$

Three types of proton conducting electrolytes are being explored: solid acids, oxides and composite electrolytes, which typically operate at temperatures between 500 and 800 K. For oxide conducting SOELs, zirconia- or ceria-based electrolytes are the most popular. Zirconia-based electrolytes show good chemical stability, but low electrochemical performance, while ceria-based electrolytes exhibit low stability, but high electrochemical performance. Temluxame et al. [81] suggested a ceria doped zirconia electrolyte, that showed low activation energy and high ionic conductivity, while performance decay rate was low compared to separate zirconia- or ceria-based electrolytes.

Temluxame et al. also investigated the influence of temperature on the ionic conductivity of oxide conducting membranes and found that with increasing operating temperature, the ionic conductivity also increased. Haile et al. [31] found a similar relation for proton conducting electrolytes. The operation of these electrolysers at elevated temperatures is thus advantageous for the material's ionic conductivity and therefore, up to a certain limit, for its Faradaic efficiencies [11]. Faradaic efficiencies are thermodynamically limited due to ammonia degradation and hydrogen formation at the cathode at elevated temperatures [21]. Finally, SOELs are still in the research stage and more research is required to improve the cell's durability.

2.3.6. Anion exchange membrane electrolysers

AEMELs combine the advantages of alkaline and PEM electrolysis. In this last type of electrolyser that will be discussed here, the two electrodes are separated by an anion exchange membrane that is able to transport OH^- anions. The oxidation and reduction reactions are equivalent to those for alkaline electrolysis, and Figure 2.7d depicts a schematic diagram for AEMELs.

Advantages of an AEMEL is its use of cheaper catalyst materials, similar to AEL, its resistance to product crossover due to dense membranes and its dynamic operation like PEMELs. However, this technology's ionic conductivity and chemical stability (mainly due to lower membrane stability) are inferior to that of AELs and PEMELs and advancements are needed in this technology [44, 55].

2.4. Separation technologies

This section deals with different separation technologies for the separation and purification of products and unconverted reactants. The compositions of the product streams depend on the type of electrolytic cell and the cross-over of reactants and products. In an electrolytic cell, diffusivity, or cross-over, of components depends on operating temperature, membrane thickness, pressure and concentration gradients, and flow rates [61, 62]. Cross-over is generally undesired, since it decreases efficiencies. However, small cross-overs usually go hand-in-hand with an increase in concentration and ohmic resistances, and thus higher overpotentials [1]. Consequently, a balance needs to be found between cross-overs and the overpotential. For this section, the separation of products streams for an electrolytic cell will be analysed and cross-overs are neglected, resulting only in the presence of reactants and products on the side of the cell where they are consumed or produced.

2.4.1. Ammonia purification

The cathodic product stream consists of different components, depending of the cell type, but generally consists of ammonia, unreacted nitrogen, hydrogen that is formed as a side product and water. The concentration of hydrogen in the cathodic product stream depends on the Faradaic efficiency. In the classical Haber-Bosch process, ammonia is separated by condensation. Other technologies that have been studied and tested are absorption and separation by membranes.

Condensation

Separation by condensation relies on the relative volatilities of the components that are present in the feed stream. In the Haber-Bosch process, a pressurised stream leaving the reactor is cooled and

enters a flash column at 50 K and around 140 bar [78]. Due to a sudden pressure decrease in the flash column, more volatile components, mainly nitrogen and oxygen gas, enter the vapour phase and will leave the column at the top. The liquid leaving at the bottom of the flash column is rich in ammonia and can be flashed another time to increase its quality, or is directly stored in a cooled or pressurised ammonia tank [64]. Nitrogen and hydrogen are compressed, heated and recycled back into the reactor, requiring a significant amount of energy [72]. A purge is necessary to prevent build up of impurities. Additionally, a membrane may recover and recycle valuable hydrogen from the purge, if this is cost and energy efficient [72]. For electrochemical ammonia synthesis from nitrogen and water however, hydrogen can not be redirected to the cell along with nitrogen and needs to be separated.

Electrochemical ammonia synthesis is conducted at lower pressures and therefore requires compression and cooling before flash separation. Kugler et al. [40] modeled electrochemical conversion to ammonia in a PEMEL cell, followed by compression, cooling and distillation of the cathodic product stream to achieve product purities of 99.5%. The first flash column facilitates separation of ammonia from hydrogen and nitrogen. A second column ensures separation of hydrogen and nitrogen. This separation process is very energy demanding and requires an energy input of around 1 kWh per kg of produced ammonia, which translates to around 8% of the total energy input for electrochemical ammonia production. Gomez et al. [29] compresses and cools the cathodic stream to 11 bar and 271 K. Consecutively, a flash drum provides ammonia with a purity of 99.9%. Based on Aspen Plus simulations, this purification process requires an energy input of 0.9 $kWh \cdot kg_{NH_3}^{-1}$.

Absorption

A second method for separation of ammonia is through absorption. This technology is based on the different absorption capacities of the different feed stream components. For Haber-Bosch processes, this enables the fast removal of ammonia, without large pressure or temperature differences [77]. This allows the reaction to operate at lower pressures, while ammonia formation rates are kept high.

Malmali et al. [50] has investigated a reaction-separation process with absorption of ammonia on calcium chloride at an absorption temperature of 460 K and a desorption temperature of 600 K. In this study, ammonia was formed in a Haber-Bosch process. Ammonia formation and absorption took place concurrently, thereby keeping the mole fraction of ammonia at a minimum and the ammonia formation rate at a maximum. Consequently, it was possible to produce ammonia rapidly at pressures as low as 25 bar.

Due to operation at relatively low pressures, separation by absorption is also interesting for electrochemical ammonia synthesis, although this has not been studied extensively yet. In another reasearch article from Malmali et al. [51], ammonia showed high absorption capacities on magnesium chloride and calcium bromide at 420 K and 4 bar. These operating conditions can be interesting for combination with electrochemical ammonia synthesis, eliminating the need for pressurisation of the separation stream.

Membranes

Separation by membranes is the last ammonia separation technology that will be discussed here. Separation by membranes is based on the different gas diffusivities and permeabilities of ammonia, hydrogen and nitrogen. Wei et al. [94] investigated the separation of ammonia by zeolitic imidazolate frameworks (ZIF) membranes. Due to the polar-polar interaction between ammonia and the membrane, ammonia was preferentially adsorbed. Moreover, ammonia is a lighter molecule than nitrogen, and therefore its gas diffusivity is larger than that of nitrogen, leading to good selectivities for NH_3/N_2 separation. However, selectivities for NH_3/H_2 separation were low due to fast hydrogen diffusivity. Advantages of separation by membranes are its operation at near ambient temperature and at reduced pressure (< 30 bar). Nonetheless, improvements in selectivity are crucial for wide-scale use of this technology.

2.4.2. Water treatment

The anodic product stream mainly consists of water and oxygen, the latter being formed as a by-product. The condensation temperatures of water and oxygen lie far apart and can be separated by condensa-

tion at near ambient conditions. Figure 2.8 shows the solubility of oxygen in pure water for different temperatures and pressures. The solubility of oxygen decreases with pressure and temperature, and lies around $1.152 \cdot 10^{-3}$ mol $\cdot$ kg^{-1} at 303 K and 1 bar [27].

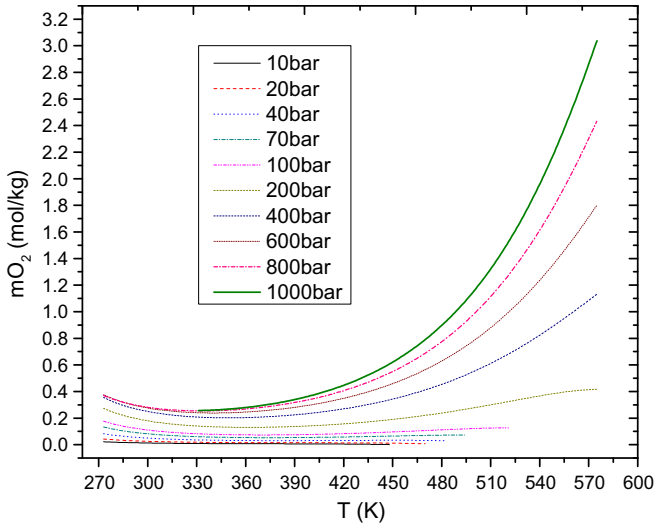

Figure 2.8: Solubility of oxygen in pure water for different temperatures and pressures. Reprinted from reference [27].

Kugler et al. [40] found that simple condensation of the anodic product stream was sufficient to achieve oxygen and water purities of 99.5%. Oxygen is a valuable by-product and can be sold for medicinal or industrial purposes. Oxygen is used, for instance, in steel production, where a purity of 95 vol% is required for iron ore treatment via the blast furnace route, and a purity of 99.5 vol% for the basic oxygen furnace route [37]. Another option is to fuel a fuel cell with oxygen and hydrogen (from the cathodic side) to provide electricity for the electrolytic cell [24].

2.5. Conclusion

Ammonia is essential for the production of fertilisers and can act as an energy vector, thereby providing a means of energy storage. For these reasons the demand for ammonia is likely to keep increasing in the coming years, while the energy consumption and carbon dioxide emissions of the currently used ammonia production process, the Haber-Bosch process, are alarming. Electrochemical ammonia synthesis is a promising alternative, which is able to utilise renewable energy for the production of ammonia from water and nitrogen.

To ensure a sustainable and energy efficient process, pre-treatment of the raw materials, the cell's performances and product separation have to be taken into account. For pre-treatment of the raw materials (air and water) energy consumption and compatibility with sustainable energy sources have to be taken into account. The performance of the electrochemical cell is mainly dependent on the ammonia formation rate, the Faradaic efficiency and the cell potential, which in turn are dependent on the electrolyte, electrodes, current and operating temperature. Ultimately, a trade-off will need to be made between these different factors. Finally, for the separation and purification of ammonia, the required purity and energy consumption need to be taken into account. For water purification on the other hand, simple condensation is considered adequate for this application.

2.5.1. Research questions

Following on this literature review and with the intention of investigating and designing an electrochemical ammonia synthesis process, the following research question and subquestions have been defined:

Research question:

Under what range of operating conditions is an electrochemical ammonia synthesis process competitive with a Haber-Bosch plant that produces 1,500 tonnes of ammonia per day in terms of energy consumption?

Subquestions:

- What pre-treatment and separation steps for electrochemical ammonia synthesis are the least energy consuming?
- What type of electrolyser is best suited for industrial electrochemical ammonia synthesis that is competitive with a Haber-Bosch process?
- Within what range of current, potential and Faradaic efficiency must an ammonia producing electrolyser operate to be competitive with the Haber-Bosch process?
- How are the energy efficiencies influenced by the electrolyser parameters?
- How is the ammonia production rate influenced by the electrolyser parameters?

3

Method

Medium size ammonia production plants have a capacity of 400,000 to 600,000 tonnes of ammonia production per year [75]. In order to compete and be comparable to current Haber-Bosch plants, a design will be made with a capacity of 550,000 tonnes per year, which is equal to 1,500 tonnes of ammonia per day. In this chapter, the options for, consecutively, pre-treatment, electrolysis and separation units are explored. Cryogenic distillation and PSA are considered and modeled as ASUs. An AEL and a PEMEL are designed as electrolysers for ammonia synthesis. Distillation and flash separation are modeled for the separation of ammonia from other (by-)products. This chapter ends with four overall process diagrams that are possible options for the production of ammonia via either an AEL or a PEMEL.

Aspen Plus® (further referred to as Aspen) is used to model the chemical processes and to determine the energy consumption of the separate process units in chapter 4. MATLAB® (further referred to as Matlab) is used to solve the set of partial differential equations that the describe the adsorption process.

3.1. Pre-treatment of air

Three air separation technologies, such as membrane separation, cryogenic distillation and PSA have been suggested for producing high purity nitrogen required for the synthesis process. Membrane separation technologies are not yet able to provide sufficient flow rates (see section 2.2) and are not considered further in this study. Cryogenic distillation and PSA, which are well established in industries, are designed to provide 99.9 mol% purity nitrogen. For both ASUs, an air intake consisting of 78 mol% N_2 and 22 mol% O_2, at ambient temperature and pressure, is assumed.

3.1.1. Cryogenic distillation

The cryogenic distillation column is designed to separate nitrogen and oxygen at a temperature of 90 K and a pressure of 6 bar. The Peng-Robinson equation of state is chosen as thermodynamic property model, which correlates well with experimental data for nitrogen and oxygen [89]. The feed stream is dry air, which is compressed and cooled to achieve the right pressure and temperature (see Figure 3.1). The ideal number of trays, feed stage, reflux ratio and distillate to feed ratio have been determined by sensitivity analyses in Aspen and are as follows:

- Number of stages: 45
- Feed stage: 10
- Reflux ratio: 0.6
- Distillate to feed ratio: 0.7

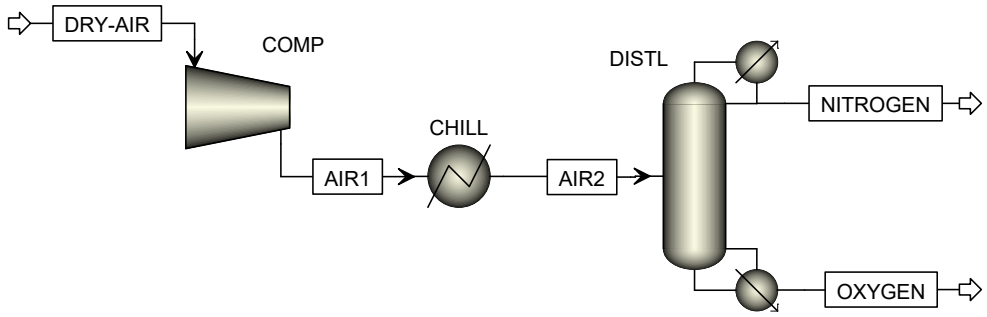

Figure 3.1: Cryogenic distillation for nitrogen generation, modeled in Aspen Plus.

3.1.2. Pressure Swing Adsorption

Commonly used adsorbents in PSA for nitrogen generation are carbon molecular sieves (CMS), which is selected as adsorbent material in the model [6, 35]. An adsorption column is not readily available in Aspen. Therefore, the adsorption equilibria of oxygen and nitrogen are modeled in a Matlab subroutine. The following assumptions are made:

- The system is isothermal.
- The adsorption equilibrium is linear and is described by Henry's adsorption isotherm.
- The mass transfer rate of a component in the gas phase to the adsorbed phase is expressed by a linear driving force (Equation 3.3).
- The flow velocity of the gas mixture varies along the length of the column and is expressed by Equation C.4.
- At t = 0 the concentration in the gas phase and adsorbed phase of both components in the column is zero.

The concentration of both components (C_i) at a certain time (t) and location in the column (z) can be found by solving the following material balance for nitrogen and oxygen (i = nitrogen, oxygen):

$$\frac{\delta C_i}{\delta t} - D_L \frac{\delta^2 C_i}{\delta z^2} + v \frac{\delta C_i}{\delta z} + C_i \frac{\delta v}{\delta z} + \frac{1-\epsilon}{\epsilon} \frac{\delta q_i}{\delta t} = 0 \tag{3.1}$$

Where D_L is the axial dispersion coefficient, v is the gas flow velocity, ϵ is the adsorption bed voidage and q_i is the amount of adsorbed nitrogen or oxygen.

The overall material balance correlates the total amount of components in the gas phase and in the adsorbed phase:

$$C_{tot} \frac{\delta v}{\delta z} + \frac{1-\epsilon}{\epsilon} \sum_i \frac{\delta q_i}{\delta t} = 0 \tag{3.2}$$

The mass transfer rate describes the rate at which either of the components is adsorbed:

$$\frac{\delta q_i}{\delta t} = k_i (q_i^* - q_i) \tag{3.3}$$

Where k_i is the linear driving force (LDF) of each component and q_i^* is the equilibrium adsorption concentration of component i. A linear adsorption equilibrium, with adsorption constant K_i, has been assumed and is described by:

$$q_i^* = K_i C_i \tag{3.4}$$

Boundary conditions:

$$C_{N_2}(z=0,t) = C_{N_2,in}, \qquad C_{O_2}(z=0,t) = C_{O_2,in}$$
$$v(0,t) = v_{in} \tag{3.5}$$

Initial conditions:

$$C_{N_2}(z,t=0) = 0, \qquad C_{O_2}(z,t=0) = 0$$
$$q_{N_2}(z,t=0) = 0, \qquad q_{O_2}(z,t=0) = 0 \tag{3.6}$$

The adsorption column (see Figure 3.2) is modeled as a cylinder with length L and an area A that is constant over its length. Filtered ambient air enters the column at z = 0 with a molar flow rate F_{in} and a velocity v_{in}. The adsorption column operates at a temperature T and pressure p. The column is discretised over its length into space steps with length Δz and over time with time steps of Δt using the Euler backward method for first derivatives and a central difference scheme for second derivatives. The discretisations can be found in Appendix C.

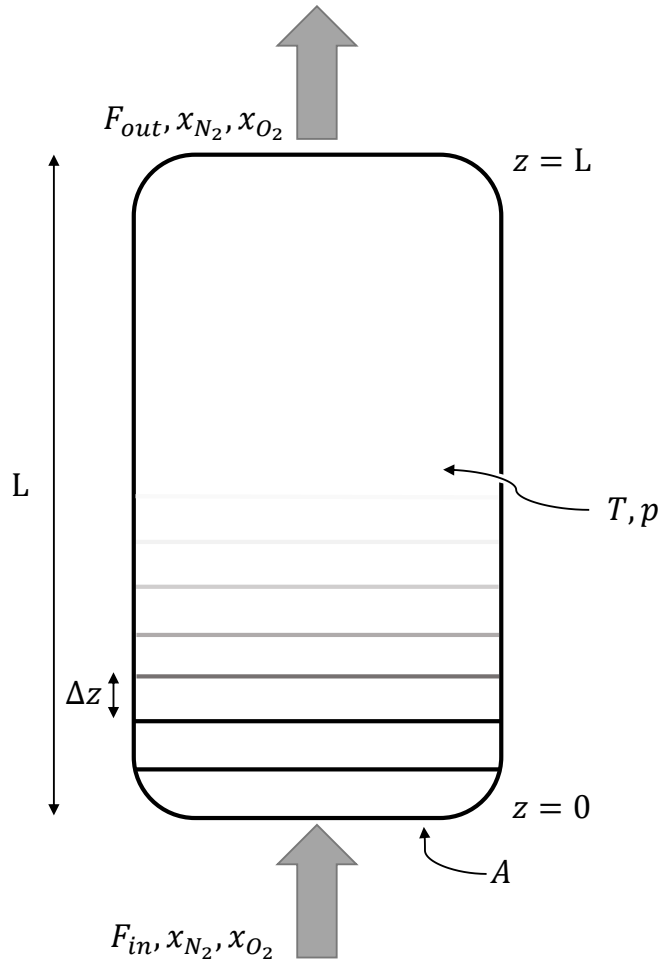

Figure 3.2: Discretisation of the PSA column.

The concentrations of both components vary in time and space and therefore the aforementioned set of equations (Equation 3.1 to Equation 3.4) also vary in time and space. For each point in time and space, a different solution to this set of equations can be found. The parameters that are used for finding the solution to the set of equations are shown in Table 3.1.

Matlab is unable to be directly coupled to Aspen. However, Excel can be used as mediator between these two to exchange information as can be seen in Figure 3.3. The adsorption column is modeled as a 'User block' with variables as in Table 3.1 that can be adjusted in Aspen. The calculations for the

Table 3.1: Parameters in PSA model [70, 72].

Parameter	Value
Axial dispersion coefficient, D_L ($m^2 \cdot s^{-1}$)	$4.876 \cdot 10^{-4}$
Bed voidage, ϵ (-)	0.4
Adsorption equilibrium constant nitrogen, K_{N_2} (-)	8.9
Adsorption equilibrium constant oxygen, K_{N_2} (-)	9.25
LDF constant nitrogen, k_{N_2} (s^{-1})	$7.62 \cdot 10^{-3}$
LDF constant oxygen, k_{N_2} (s^{-1})	$44.71 \cdot 10^{-3}$
Length column, L (m)	3.5
Area column, A (m^2)	0.56745
Operating temperature column, T (K)	298
Operating pressure column, P (bar)	9.4
Adsorption cycle time, t_a (s)	30

adsorption column are executed in Matlab and finally the results for the product streams are communicated back to Aspen via Excel.

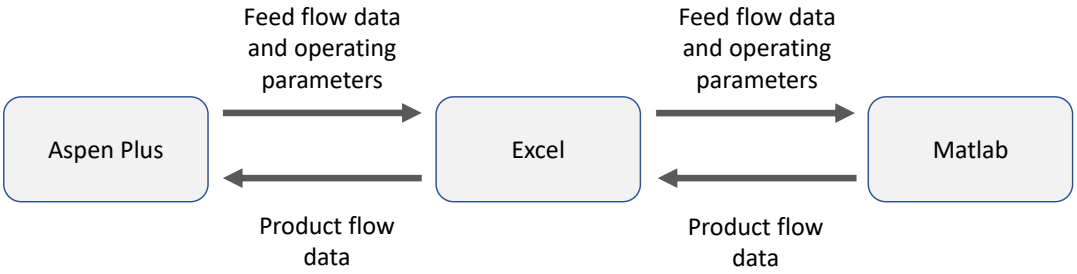

Figure 3.3: Communication between Aspen, Excel and Matlab in the process modeling of the adsorption column.

In practice, the PSA system looks like in Figure 2.3, with two adsorption columns that are active alternatively. In this study, however, only the active column is shown in the process diagram and the desorption of the adsorbent is not modeled as shown in Figure 3.4.

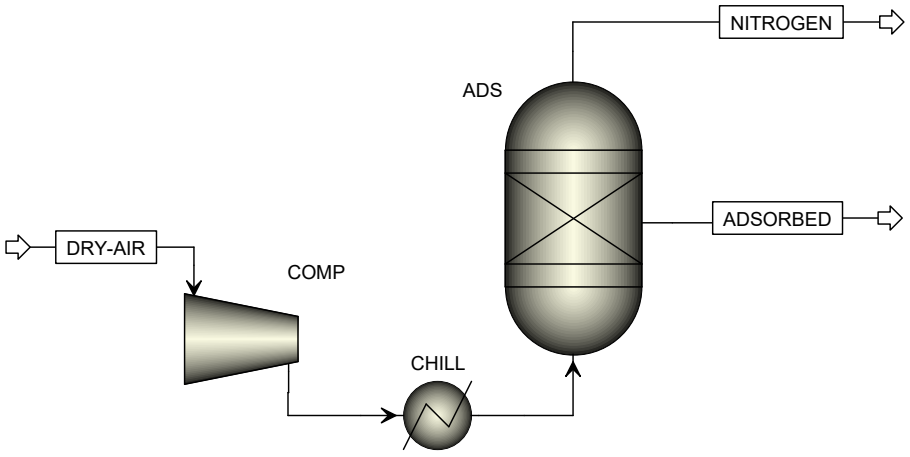

Figure 3.4: Pressure Swing Adsorption for nitrogen generation, as modeled in Aspen Plus.

3.2. Electrochemical cell

Four different types of electrochemical cells were described in subsection 2.3.2. However, Faradaic efficiencies of SOELs are currently limited and AEMELs need advancements in their ionic conductivity and chemical stability for this technology to be technical feasible. AEL and PEMEL are currently the

most promising water electrolysers [11]. Whether they are better able to synthesise ammonia than SOEL and AEMEL needs to be proven in the future, but this is outside the scope of this research. Therefore, an AEL and a PEMEL are modeled in this section.

The electrochemical cell is considered as a 'black box', this means that the cell is not modeled in detail, and heat and mass transfer, flow patterns and the cell set up are not taken into account. In Figure 3.5 the electrochemical cell is represented as the black box, with a certain temperature, pressure, cell potential, and a current that depends on the required ammonia formation rate, with incoming streams as the feed streams and the outgoing streams containing the products and by-products.

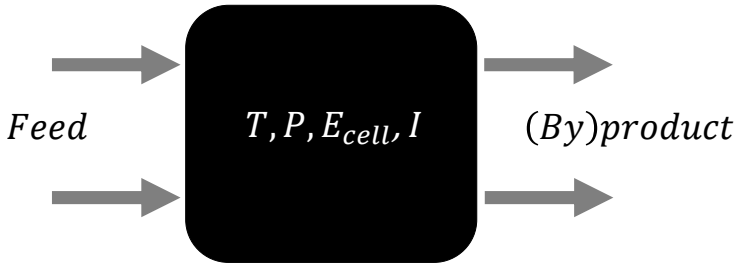

Figure 3.5: Electrochemical cell considered as a black box in the simulation with pre-defined temperature, pressure and cell potential and a current that needs to be determined.

Buttler et al. investigated current state-of-the-art water electrolysers and gave a summary of their operation parameters [11]. In this study, the A485 Hydrogen electrolyser is taken as a reference for the AEL and the Siemens SILYZER 200 is taken as a reference for the PEMEL [60, 74]. The average temperature of both cells have been set at 353 K. The AEL operates at atmospheric pressure and the PEMEL operates at a pressure of 30 bar. We assume a single-pass conversion of 25%, since at lower conversions the process is unlikely to be economically feasible [92].

The electrochemical cells have two feeds, a nitrogen feed and a water or potassium hydroxide solution for a PEMEL or an AEL cell respectively. One of the streams leaving the AEL contains the volatile components produced in the cell, while the other stream contains dissolved ammonia in a KOH solution, as can be seen in Figure 3.6a. The two streams leaving the PEMEL are the streams leaving the anodic and the cathodic side of the cell, which consist of oxygen and water, or ammonia, hydrogen and nitrogen respectively (see Figure 3.6b). It is assumed that no water is present in the cathodic product side, since the permeability of water through the membrane is small and at high current densities water is directly consumed at the electrodes [95].

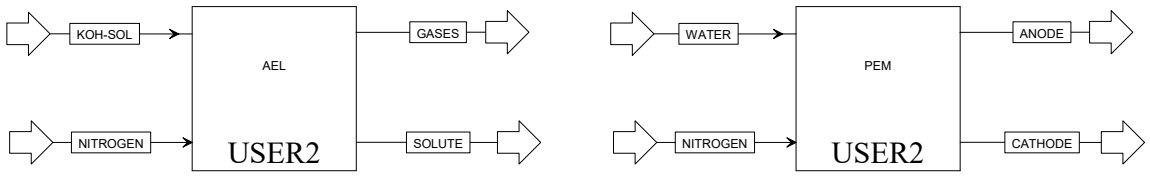

(a) AEL (b) PEMEL

Figure 3.6: Electrochemical cells simulated in Aspen Plus.

The electrochemical cell itself is modeled as a user block, for which the feed details and cell specifications are collected, send to an Excel file where calculations are made for the product streams and finally the calculated values are send back to Aspen to define the product streams. The current required for the production of a certain amount of ammonia is described by Faraday's law:

$$I = \frac{r_{NH_3,cell} \cdot n \cdot F}{FE} \tag{3.7}$$

Where FE is the Faradaic efficiency. Where $r_{NH_3,cell}$ is the ammonia formation rate inside the cell. Note that this value is larger than the production rate of 1,500 tonnes per day due to ammonia loss in the

separation process. n represents the amount of moles of electrons required for the formation of one mole of ammonia, which is equal to three.

It is assumed that the only side-product is hydrogen (with n = 2). Therefore, the amount of hydrogen that is produced, is calculated as:

$$r_{H_2} = \frac{I \cdot (1 - FE)}{n \cdot F} \tag{3.8}$$

3.3. Separation of ammonia

In this subsection, the separation of ammonia from an electrolyte and the separation of ammonia from a gaseous mixture of hydrogen and nitrogen are modeled. The first is applicable for the solute stream coming from the AEL, while the second is relevant for the cathodic product stream of a PEMEL.

3.3.1. Distillation

The solute stream consists of a 1 M KOH solution containing ammonia at atmospheric pressure and 353 K. Ammonia and the electrolyte are separated using a distillation column which is modeled in Aspen. Since the process involves the separation of ammonia from an electrolyte, a special thermodynamic property model is needed to describe the relation between the different components. The Electrolyte NRTL/Redlich-Kwong model has been proven to accurately describe the interaction between the concerned components at atmospheric pressures and is therefore chosen as thermodynamic property model [52].

The solute stream from the AEL enters the distillation column as shown in Figure 3.7a. In the column, ammonia is separated from the electrolyte and leaves at the top, this stream is called 'ammonia'. The bottom stream contains the electrolyte and some unseparated ammonia. A distillation column has been designed for different concentrations of ammonia in the solute stream, the specifications of these columns can be found in Appendix D.

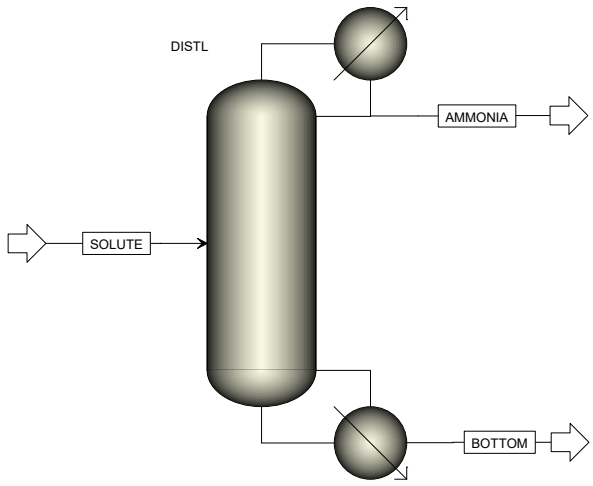

(a) The distillation of ammonia from a KOH solution.

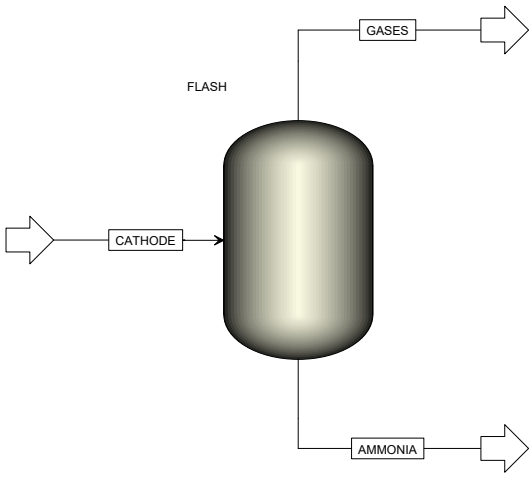

(b) The separation of ammonia from a gaseous mixture by a flash drum.

Figure 3.7: Two technologies for the separation of ammonia from the electrochemical cell's product stream, modeled in Aspen Plus.

3.3.2. Flash separation

The cathodic product stream from the PEMEL consists of ammonia, nitrogen and hydrogen, at 30 bar and 353 K. The product stream is pressurised, which suggests flashing at an intermediate pressure to allow for pressurised storage of ammonia. The bottom product of the flash drum contains at least 99.9

mol% purity ammonia and the stream leaving the top of the flash drum contains hydrogen and nitrogen. Figure 3.7b shows a diagram of the flash separation in a PEMEL based process.

For the modeling of the flash drum in Aspen Plus, the Peng-Robinson equation of state is chosen, which has been proven to well estimate the relation between ammonia, nitrogen and hydrogen [39, 89].

3.4. Overall process diagrams

The separate process units are combined to four different overall process diagrams, shown and elaborated in this section. A complete overview of all streams, with mass and energy flows, can be found in Appendix E. Note that all heaters and chillers are modeled as separate units. Thus no heat integration has been applied in this study.

3.4.1. Process diagrams for an alkaline electrolyser

For the alkaline electrolyser, two combinations can be designed for the entire production process. The first option consists of a cryogenic distillation column for the generation of nitrogen, followed by an AEL and another distillation column for the separation of ammonia from the electrolyte (see Figure 3.8). The second option consists of a set of PSA columns. However, only one column is modeled (ADS in the process diagram). In order to attain the appropriate product flows while only one column is modeled, the air feed (stream AIR2) is divided by the total number of PSAs. The visible adsorption column can be considered as one PSA in a number of parallel connected PSAs. After the adsorption sub-process, the streams leaving the adsorption column are multiplied by the number of PSAs, ensuring the correct flow of nitrogen. The ASU is followed by an AEL and again a distillation column for the separation process (see Figure 3.9). In both cases ammonia is compressed to a pressure of 10 bar and cooled down to a temperature of 298 K after separation, which are conventional storage conditions for ammonia [66].

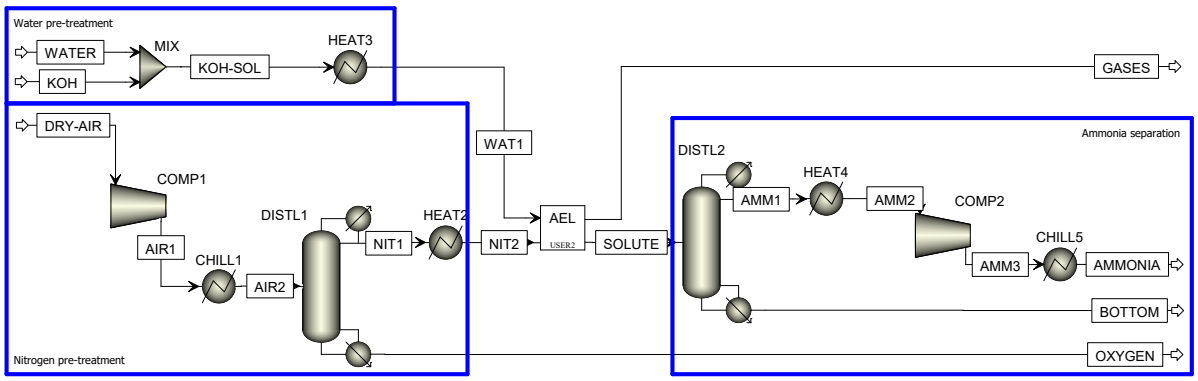

Figure 3.8: Overall process diagram for an AEL with cyrogenic distillation for nitrogen distillation.

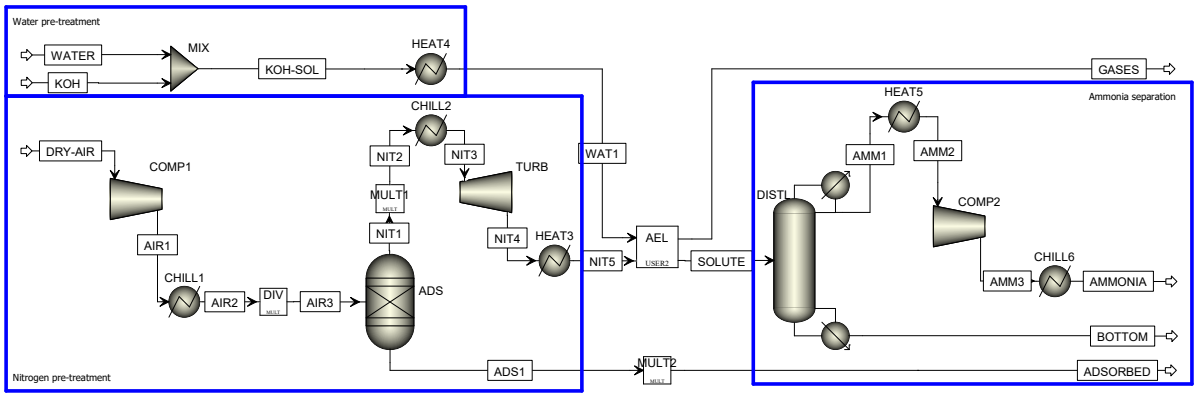

Figure 3.9: Overall process diagram for an AEL with PSA for nitrogen generation.

3.4.2. Process diagrams for a PEM electrolyser

Also for the PEMEL two combinations of production processes can be designed. The first one involves a distillation column for nitrogen generation, followed by a PEMEL cell and a flash drum for the separation of ammonia (see Figure 3.10). For the second option the distillation column is replaced by a set of adsorption columns (similar to the case with an AEL) for the generation of nitrogen (see Figure 3.11). Since the PEMEL cell operates at 30 bar and the flash drum at 15 bar, the cathodic product stream does not need to be compressed, but can be stored directly after separation.

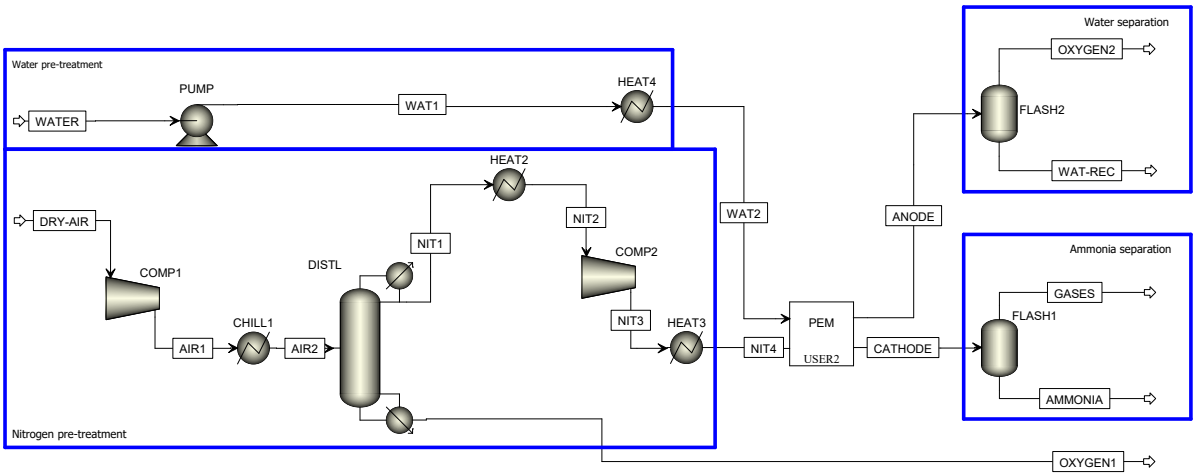

Figure 3.10: Overall process diagram for a PEMEL with cryogenic distillation for nitrogen generation.

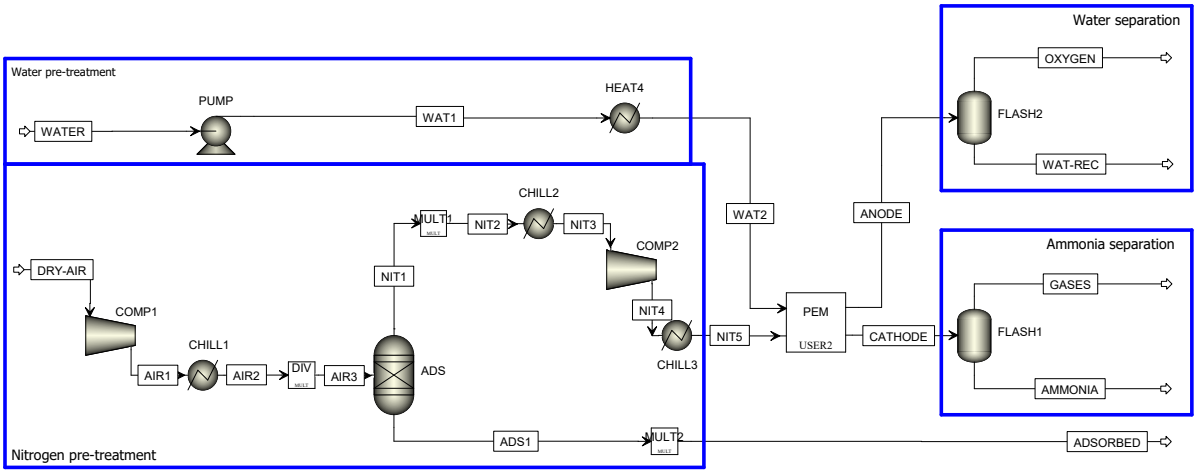

Figure 3.11: Overall process diagram for a PEMEL with PSA for nitrogen generation.

4

Results

In this chapter, the results of the different simulations are shown for the production of a process plant that is able to produce 1,500 tonnes of ammonia per day. First, cryogenic distillation and PSA for the generation of nitrogen are compared and their optimal operating parameters are defined. Subsequently, distillation and a flash drum for the separation of ammonia from the product stream are compared, their operating parameters and the optimal ammonia concentration in the product stream are determined. Afterwards, four combinations of pre-treatment and separation steps are created and evaluated. Finally, the relation between the cell's operating parameters and its energy consumption is calculated, and the operating parameters at which the entire system is competitive with a Haber-Bosch process are determined.

4.1. Pre-treatment analysis

4.1.1. Cryogenic distillation

After allocating the operating parameters from subsection 3.1.1 and the feed stream values from section 3.1 to a distillation column in Aspen, the simulation can be carried out. The energy consumption per kilogram of separated nitrogen is presented in Table 4.1.

Table 4.1: Energy consumption of a cryogenic distillation unit for nitrogen generation.

Utility	Function	Energy consumption (kWh · $kg_{N_2}^{-1}$)
COMP	Air compressor	0.114
CHILL	Air cooler	0.279
DISTL (Reboiler)	Distillation reboiler	0.080
DISTL (Condenser)	Distillation condenser	0.089
Total		0.56

4.1.2. Adsorption column

Figure 4.1b shows the concentration of each component in the gas phase along the length of the adsorption column at an intermediate time step t. As can be seen, oxygen is gradually removed from the gas phase and almost no oxygen leaves the end of the column. The concentration of nitrogen in the gas phase increases in the first half of the column. This is due to the fact that at earlier time steps nitrogen was adsorbed at these locations (see Figure 4.1a), but is now being desorbed to accommodate the adsorption of oxygen, which has a higher adsorption equilibrium constant. In the remainder of the column, more nitrogen is adsorbed since the adsorbent is not fully saturated here. Finally, at time step t, a product stream leaves the column at z = L with $C_{N_2}(z = \mathrm{L}, t)$ and $C_{O_2}(z = \mathrm{L}, t)$.

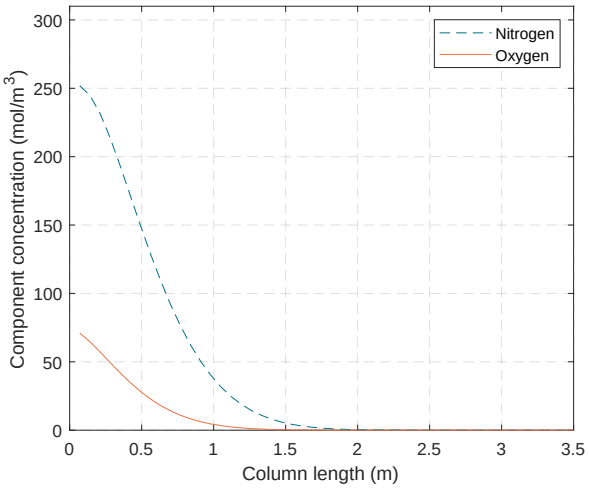

(a) At time step 3 (t = 1.8 s)

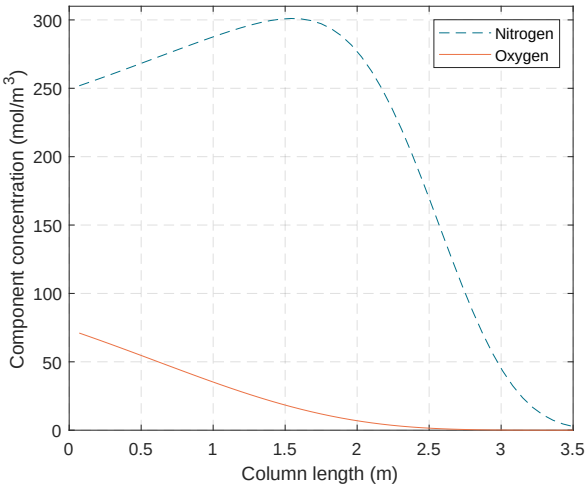

(b) At time step 16 (t = 9.6 s)

Figure 4.1: The concentration of each component at intermediate time steps along the length of the adsorption column.

The nitrogen purity of the stream leaving the adsorption column changes during one cycle. However, the nitrogen is collected in a well-stirred storage tank and therefore the stream leaving the storage tank has a constant concentration which is calculated as:

$$C_{N_2} = \frac{1}{N_t} \sum_{t=0}^{t=t_a} C_{N_2}(z = \mathrm{L}, t) \tag{4.1}$$

Operating parameters that need to be determined are the operating pressure, operating temperature and adsorption cycle time. These are optimised using the Model Analysis Tool in Aspen until the required nitrogen purity is achieved and the nitrogen recovery is at least 10 mol%. The pressure dependency of the nitrogen purity and nitrogen recovery are displayed in Figure 4.2a. The nitrogen purity increases with increasing pressure, but its recovery decreases with a rise in pressure. The opposite can be observed in the plot for the temperature dependency (see Figure 4.2b) . Here, the nitrogen purity declines with increasing temperature, while the nitrogen recovery becomes larger as the temperature rises.

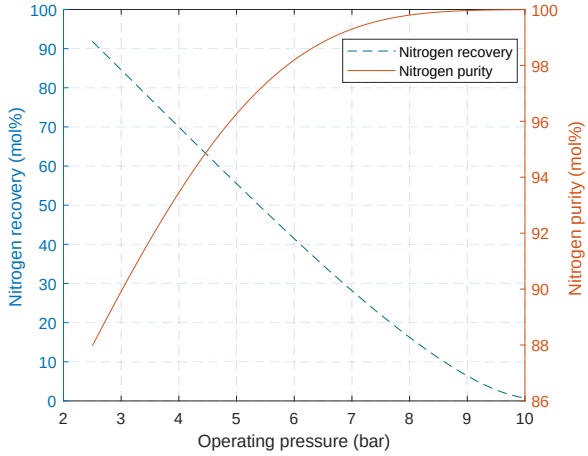

(a) Pressure dependency (at T = 298 K)

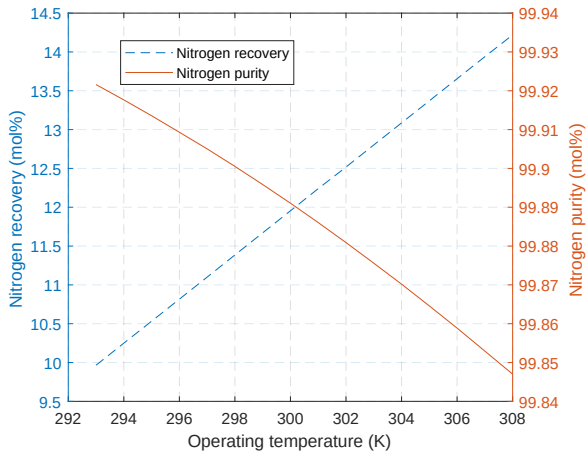

(b) Temperature dependency (at p = 9.4 bar)

Figure 4.2: Nitrogen purity and nitrogen recovery for different operating parameters.

The optimal operating temperature and pressure are determined by choosing a combination of these two variables that gives a nitrogen purity of at least 99.9 mol%. This purity is achieved at a pressure of 9.4 bar and a temperature of 298 K. To attain this pressure, dry air is compressed before entering the column, causing the temperature to rise. Therefore, the air stream is cooled down to a temperature of 298 K. The adsorption cycle time t_a is set at 30 s, which is comparable to earlier studies and in which time most oxygen in adsorbed [6, 70].

The energy consumption for the production of nitrogen via this PSA process was found to be equal to 1.82 kWh $\cdot$ $kg_{N_2}^{-1}$.

Finally, the assumption of a zero pressure drop is checked by calculating the pressure drop using Ergun's equation:

$$\frac{dp}{dz} = -150\frac{(1-\epsilon)^2}{\epsilon^3}\frac{V\cdot\mu}{A_c\cdot D_p^2} - 1.75\frac{(1-\epsilon)}{\epsilon^3}\frac{V\cdot m}{D_p\cdot A_c^2} \tag{4.2}$$

The parameters that are used for the calculation are summarised in Table 4.2. The resulting pressure drop is equal to $1.05\cdot 10^4$ Pa per meter column. For a column length of 3.5 m (as in this study), the pressure drop over the entire column is 0.37 bar.

Table 4.2: Parameters used in Ergun's equation for the calculation of pressure drop in a reactor, values from own PSA simulation (subsection 3.1.2).

Symbol	Description	Value
ϵ	Bed voidage	0.4 [71]
V	Volumetric flow rate	0.223 $m^3\cdot s^{-1}$
μ	Dynamic viscosity (air)	$1.81\cdot 10^{-5}$ Pa $\cdot$ s [19]
A_c	Bed cross sectional area	0.56745 m^2
D_p	CMS particle diameter	0.003 m [69]
m	Mass flow rate	2.60 kg $\cdot$ s^{-1}

4.2. Separation analysis

4.2.1. Distillation

The distillation column for separating ammonia from an electrolyte is modeled for different concentrations of ammonia in the 1 M KOH solute product stream with the column specifications in Table D.1. Table 4.3 gives an overview of the ammonia recovery and the energy consumption of the distillation process for different ammonia concentrations, obtained from Aspen. These values are also plotted in Figure 4.3. It can be seen in this figure that the energy requirements for the distillation column increase rapidly at concentrations below 10 mol% of ammonia. It is therefore assumed necessary to achieve a concentration of at least 10 mol% of ammonia in the solute leaving the AEL. This means that an electrolyte flow rate nine times as large as the ammonia formation rate is required.

Table 4.3: Energy requirement for a separation process of ammonia from a 1 M KOH solution for different concentrations of ammonia in the cathodic product stream.

NH_3 purity (mol%)	NH_3 recovery (mol%)	Energy consumption (kWh $\cdot$ $kg_{NH_3}^{-1}$)
4	99.4	10.04
5	99.9	8.13
10	99.5	1.75
15	99.5	1.36
20	99.4	1.11

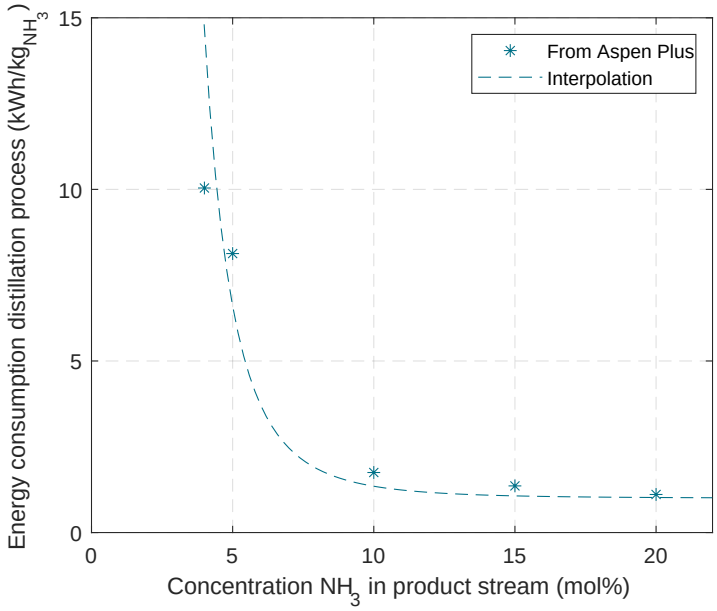

Figure 4.3: Energy requirement for the distillation of ammonia from an electrolyte for different concentrations of ammonia in the solute product stream of an AEL.

4.2.2. Flash separation

A flash separation unit is designed for different concentrations of ammonia in the cathodic gaseous product stream. The selected operating parameters and resulting energy requirements are shown in Table 4.4.

Table 4.4: Energy requirement for a separation process of ammonia from a gaseous mixture for different concentrations of ammonia in the cathodic product stream and a flash drum operating at different temperatures.

Concentration ammonia (mol%)	Operating temperature flash drum (K)	Operating pressure flash drum (bar)	Energy consumption (kWh $\cdot$ kg$^{-1}_{NH_3}$)
1	140.55	15	11.05
5	151.65	15	2.44
10	157.15	15	1.41
25	167.15	15	0.80
50	184.05	15	0.60

The energy consumption of the flash drum is plotted in Figure 4.4a. It can be observed that the energy consumption for the separation process increases radiply at concentrations below 10 mol% of ammonia. The required operation temperature of the flash drum is also plotted in Figure 4.4a and also gives an estimation for the required operation temperature of the flash drum at intermediate concentrations.

The influence of the Faradaic efficiency of the PEMEL on the separation process was studied as well. The concentration of ammonia in the cathodic product stream has been set at 10 mol%, so the Faradaic efficiency does not influence this concentration. However, the Faradaic efficiency does influence the amount of hydrogen that is produced as byproduct. The Faradaic efficiency does thus influence the $H_2 : N_2$ ratio, which influences the energy requirement for the separation of ammonia from hydrogen and nitrogen. Figure 4.4b gives the energy consumption and required operating temperature of the flash drum for different Faradaic efficiencies. It can be seen that a higher Faradaic efficiency, and therefore lower hydrogen content, requires a lower operating temperature of the flash drum and therefore a higher energy consumption. This can be attributed to the fact that the volatilities of hydrogen and ammonia are further apart and therefore less energy is required to separate these components.

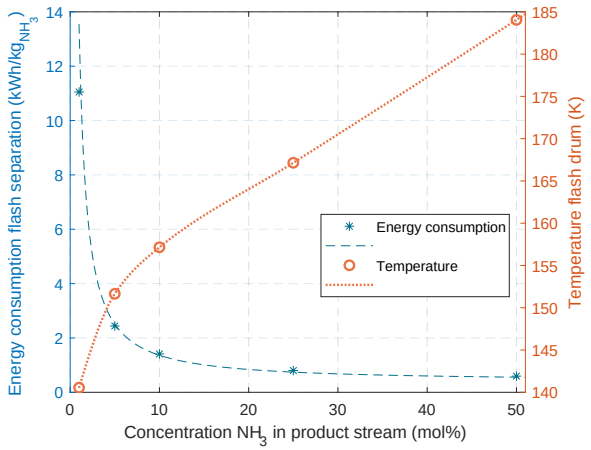

(a) Energy requirement for different concentrations of ammonia in the cathodic product stream.

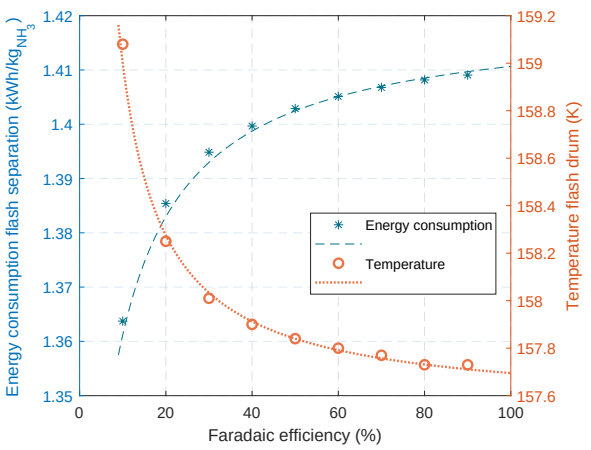

(b) Energy requirement for different Faradaic efficiencies and therefore different $H_2 : N_2$ ratios, at an ammonia concentration of 10 mol%.

Figure 4.4: Operating temperature of the flash drum and its energy requirement for the separation process of ammonia from a gaseous mixture.

4.3. Energy consumption pre-treatment and separation

The energy consumption per kilogram of produced ammmonia can be calculated by adding the energy consumption for all equipment, except for the electrochemical cell, for each of the process diagrams. The energy consumption in kWh $\cdot$ kg$^{-1}_{NH_3}$ is retrieved from Aspen and presented in Table 4.5, Table 4.6, Table 4.7 and Table 4.8.

4.3.1. Process with an alkaline electrolyser

For the options where ammonia is produced by an AEL, one of the most energy consuming steps is the distillation of ammonia and the electrolyte. It is found that the separation of ammonia from an electrolyte is energy consuming, due to the dissolved ammonia. Separation becomes even more troublesome if lower concentrations of ammonia are found in the solute stream, as was shown in subsection 3.3.1.

Table 4.5: Energy consumption of the utilities in an AEL based process with distillation for nitrogen generation.

	Utility	Function	Energy consumption (kWh $\cdot$ kg$^{-1}_{NH_3}$)
Nitrogen pre-treatment (distillation)	COMP1	Air compressor	0.38
	CHILL1	Air cooler	0.94
	DISTL1	ASU distillator	0.57
	HEAT2	Nitrogen heater	0.45
Water pre-treatment	HEAT3	Water heater	0.72
Separation (distillation)	DISTL2	Ammonia separation distillator	1.29
	HEAT4	Ammonia heater	0.38
	COMP2	Ammonia compressor	0.14
	CHILL5	Ammonia cooler	0.43
	Total		5.30

For a process where nitrogen is produced by PSA columns and ammonia is synthesised by an AEL, most energy is consumed by the first cooler. The air stream is considerably heated due to compression and needs to be cooled down again before being fed to the adsorption column. This air stream is relatively large, because the PSA has a nitrogen recovery of around 11.4 mol%, therefore requiring a

large feed to produce enough nitrogen. This causes the high energy requirements of the generation of nitrogen by PSA. Also here, the distillation of ammonia and the electrolyte requires a signification amount of energy.

Table 4.6: Energy consumption of the utilities in an AEL based process with PSA for nitrogen generation.

	Utility	Function	Energy consumption ($kWh \cdot kg_{NH_3}^{-1}$)
Nitrogen pre-treatment (PSA)	COMP1	Air compressor	3.04
	CHILL1	Air cooler	3.06
	CHILL2	Nitrogen cooler	0.002
	HEAT3	Nitrogen heater	0.15
Water pre-treatment	HEAT4	Water heater	0.72
Separation (distillation)	DISTL	Ammonia separation distillator	1.29
	HEAT5	Ammonia heater	0.38
	COMP2	Ammonia compressor	0.14
	CHILL6	Ammonia cooler	0.43
	Total		9.21

4.3.2. Process with a PEM electrolyser

For a system where nitrogen is produced via cryogenic distillation and ammonia is synthesised by a PEMEL cell, most energy is consumed by the cooling down of the air stream. However, this energy requirement is smaller than that in the case of a PSA, because the molar flow of the air stream is smaller.

Table 4.7: Energy consumption of the utilities in a PEMEL based process with distillation for nitrogen generation.

	Utility	Function	Energy consumption ($kWh \cdot kg_{NH_3}^{-1}$)
Nitrogen pre-treatment (distillation)	COMP1	Air compressor	0.38
	CHILL1	Air cooler	0.92
	DISTL	ASU distillator	0.56
	HEAT2	Nitrogen heater	0.22
	COMP2	Nitrogen compressor	0.10
	HEAT3	Nitrogen heater	0.12
Water pre-treatment	PUMP	Water compressor	0.006
	HEAT4	Water heater	0.44
Separation (flash)	FLASH	Ammonia flash separator	0.75
	Total		3.50

Also for a PEMEL cell with PSA for nitrogen generation most energy is required for the cooling down of the air stream.

It can be concluded that for both electrolysers, a process that uses cryogenic distillation as a pre-treatment step is the most optimal in terms of energy use. For a process with an alkaline electrolyser, the separation of ammonia should be done via distillation. For a process with a PEMEL, ammonia can be separated from the gaseous mixture through flash separation.

Table 4.8: Energy consumption of the utilities in a PEMEL based process with PSA for nitrogen generation.

	Utility	Function	Energy consumption (kWh · $kg^{-1}_{NH_3}$)
Nitrogen pre-treatment (PSA)	COMP1	Air compressor	3.04
	CHILL1	Air cooler	3.06
	CHILL2	Nitrogen cooler	0.005
	COMP2	Nitrogen compressor	0.15
	CHILL3	Nitrogen cooler	0.10
Water pre-treatment	PUMP	Water compressor	0.006
	HEAT4	Water heater	0.44
Separation (flash)	FLASH	Ammonia flash separator	0.75
	Total		7.55

4.4. Energy consumption electrochemical cell

The entire process should be competitive with a Haber-Bosch process in terms of energy use. This means that the energy consumption of the pre-treatment (E_{p-t}), electrolyser (E_{el}) and separation (E_{sep}) steps together should be comparable to the energy consumption by a Haber-Bosch process (E_{H-B}), which translates to around 8.8 kWh · $kg^{-1}_{NH_3}$ (see subsection 2.1.1):

$$E_{H-B} \approx E_{p-t} + E_{el} + E_{sep} \tag{4.3}$$

The efficiency of all pre-treatment and separation utilities is incorporated in the calculations made by Aspen. The electrical energy efficiency of the electrolyser is defined as the amount of power that is used to provide a current over the total power input. Electrical energy losses are mainly due to heat generation within the cell. In order to determine these losses, more information on the reactions and heat transfer in the cell needs to be known and therefore, in this study, an electrical energy efficiency of 100% is assumed.

The energy consumption for the pre-treatment and separation steps for a process with an AEL and a PEMEL have been calculated in section 4.3 and the amount of energy required by the electrolyser is calculated as:

$$E_{el} = \frac{P_{cell}}{r_{NH_3}} = \frac{U_{cell} \cdot I}{r_{NH_3}} \tag{4.4}$$

Note that the ammonia production rate used here (r_{NH_3}) is different from the ammonia formation rate ($r_{NH_3,cell}$) from Equation 3.7. $r_{NH_3,cell}$ is the rate at which ammonia is produced in the electrochemical cell, while r_{NH_3} is the rate at which ammonia leaves the entire production process, which is lower since some ammonia is lost during the separation step. In order to find the relation between the cell parameters and the ammonia formation rate, the amount of ammonia formed in the cell ($r_{NH_3,cell}$) is plotted as a function of the applied current for different Faradaic efficiencies in Figure 4.5a. As can be observed, a higher Faradaic efficiency results in an increase in ammonia formation. The applied current is also linearly related to an increase in the ammonia formation rate, described by Faraday's law (Equation 3.7).

The cell's energy requirements are linearly related to the applied current (see Equation 4.4). Thus, in order to find the relation between the cell's parameters and the energy consumption, first the required current is plotted as a function of the Faradaic efficiency, for different ammonia formation rates in the cell ($r_{NH_3,cell}$) in Figure 4.5b. The required current increases rapidly at lower Faradaic efficiencies for all $r_{NH_3,cell}$. Unless stated otherwise, in the remainder of this thesis we assume a Faradaic efficiency of 70%, since higher Faradaic efficiencies do not influence the required current drastically.

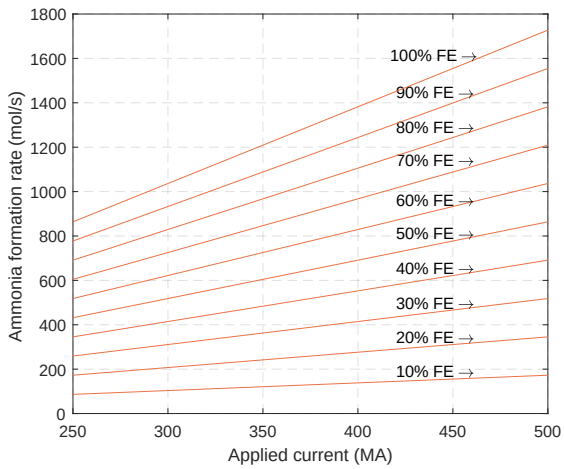

(a) The ammonia formation rate as a function of the applied current for different Faradaic efficiencies.

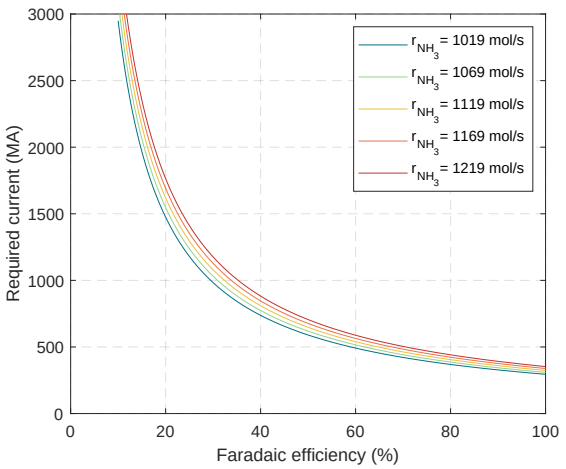

(b) Required current as a function of the Faradaic efficiency, for different ammonia formation rates.

Figure 4.5: Relation between the Faradaic efficiency, applied current and ammonia formation rate, described by Faraday's law.

For both cells, an overpotential of 0.6 V is assumed, as is predicted to be a reasonable prediction by Wang et al. [91]. This results in a cell potentials of 1.77 V.

4.4.1. Alkaline electrolyser

The ammonia recovery rate using distillation with an AEL is 99.5 mol%. To maintain an ammonia production rate of 1,500 tonnes per day, the electrochemical cell needs to achieve an ammonia formation rate of 1024.50 $\text{mol} \cdot \text{s}^{-1}$. Using Faraday's law (Equation 3.7) and a Faradaic efficiency of 70%, the required current is calculated to be 423.64 MA.

With a cell potential of 1.77 V, an electrical energy input of 12.00 $\text{kWh} \cdot \text{kg}^{-1}$ is needed for the electrochemical cell. The energy consumption for pre-treatment and separation steps in an AEL process is 5.30 $\text{kWh} \cdot \text{kg}_{\text{NH}_3}^{-1}$ (see Table 4.5). This leads to a total energy consumption of 17.30 $\text{kWh} \cdot \text{kg}_{\text{NH}_3}^{-1}$ for a process where ammonia is produced by an alkaline electrolyser.

4.4.2. PEM electrolyser

For a process with a PEMEL cell, the ammonia recovery rate for the separation step is 99.9 mol%. This results in a required ammonia formation rate of 1020.40 $\text{mol} \cdot \text{s}^{-1}$. Again, using Faraday's law and a Faradaic efficiency of 70%, the applied current should be 421.94 MA. Applying Equation 4.4 and a cell potential of 1.77 V, this results in an energy consumption of 11.95 $\text{kWh} \cdot \text{kg}_{\text{NH}_3}^{-1}$.

For the pre-treatment and separation steps in a PEMEL process, the energy consumption is 3.50 $\text{kWh} \cdot \text{kg}_{\text{NH}_3}^{-1}$ (see Table 4.7), leading to a total energy consumption of 15.45 $\text{kWh} \cdot \text{kg}_{\text{NH}_3}^{-1}$ for a process where ammonia is produced by a PEMEL.

Figure 4.6a shows the required current for different Faradaic efficiencies for an AEL and a PEMEL. The minimal current that is needed to produce the fixed amount of ammonia lies around 300 MA for both cells and increases with decreasing Faradaic efficiency. The energy consumption of the cells for different cell potentials and Faradaic efficiencies is plotted in Figure 4.6b. The cells will require at least 5 $\text{kWh} \cdot \text{kg}_{\text{NH}_3}^{-1}$, even at 100% Faradaic efficiency and the standard equilibrium cell voltage.

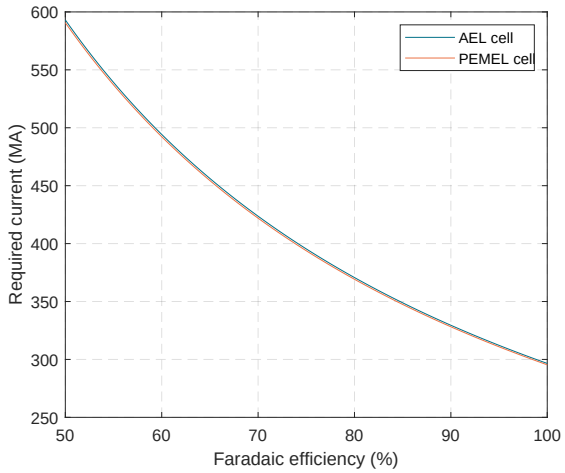

(a) Required current to achieve r_{NH_3} for different Faradaic efficiencies for an AEL and a PEMEL cell.

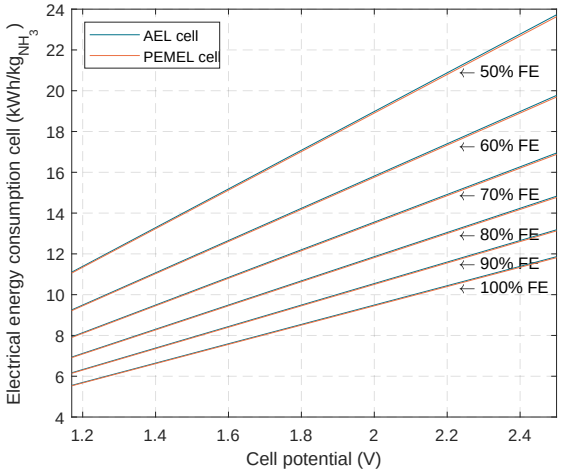

(b) Energy consumption for different cell potentials and at different Faradaic efficiencies for an AEL and a PEMEL cell.

Figure 4.6: Required current for different Faradaic efficiencies of an AEL and a PEMEL cell and the resulting electrical energy consumption of the cell at different Faradaic efficiencies and for a range of cell potentials.

In order to find the relation between the electrolyser parameters and the energy efficiency of the entire process, the energy consumption of the different processes have been calculated. Subsequently, the energy efficiency of the entire process is calculated as the LHV of ammonia over the energy consumption of the entire process, and is plotted for different cell potentials and Faradaic efficiencies in Figure 4.7a and Figure 4.7b. The overall energy efficiency declines with decreasing Faradaic efficiency and increasing cell potential. The energy efficiency of a PEMEL based process is higher at all cell potentials and Faradaic efficiencies than an AEL based process, due to a lower energy consumption of its sub-processes. At a cell potential of 1.77 V and a Faradaic efficiency of 70%, the overall energy efficiency is 29.88% for an AEL based process and 33.46% for a PEMEL based process. Even at the lowest overpotentials and a Faradaic efficiency, an overall energy efficiency of 50% is merely reached.

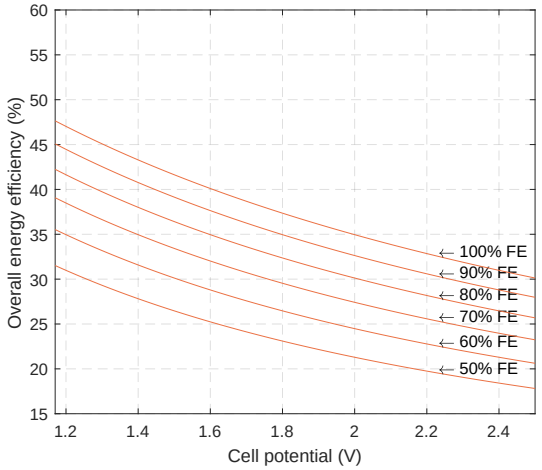

(a) Process with an AEL cell.

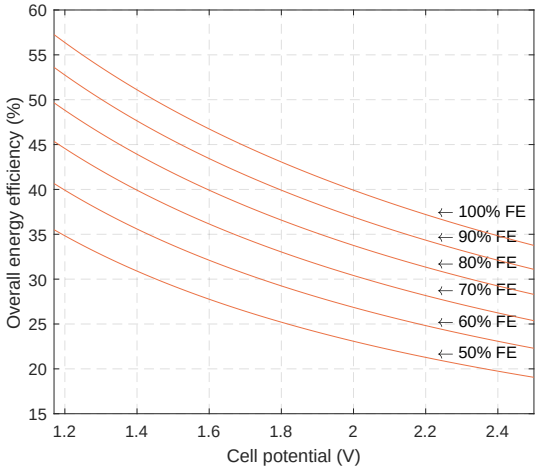

(b) Process with a PEMEL cell.

Figure 4.7: Energy efficiency for two overall ammonia production processes.

5

Discussion

5.1. Nitrogen pre-treatment

The energy consumption for nitrogen generation by cryogenic distillation, as found in our Aspen model, is 0.56 kWh $\cdot$ $kg_{N_2}^{-1}$. This is compared to the 0.42 kWh $\cdot$ $kg_{N_2}^{-1}$ found by Aneke et al. [7]. The energy consumption for the system designed by Aneke is lower, which is mainly due a better designed system with high and low pressure columns. The result found by Aneke is promising because this means that the energy consumption of the pre-treatment process can be reduced if the system is optimised.

The energy consumption for nitrogen generation via PSA is 1.82 kWh $\cdot$ $kg_{N_2}^{-1}$. For the modeling of the adsorption column, a linear adsorption equilibrium was assumed, as suggested by Sánchez et al. [72]. However, a non-linear adsorption isotherm gives a better description of the adsorption equilibrium of oxygen and nitrogen on CMS [6]. A zero pressure drop was assumed, however this pressure drop influences the assumption of a constant fluid density and therefore the fluid velocity. Also the adsorption equilibrium is influenced by a pressure difference. Nevertheless, a pressure drop of 4% (0.37 bar on a pressure of 9.4 bar) was calculated in subsection 4.1.2 and is considered small enough to not have a significant effect on the current simulation.

As was shown in section 4.3, a PSA unit for the generation of nitrogen is more energy consuming than cryogenic distillation at this scale. This same result was found by Sánchez et al., who compared membranes, PSA and distillation systems at different scales [72]. Most energy is consumed by cooling down of the large air stream that is heated due to compression to 9.4 bar. When heat integration is applied, energy from the air stream can be used to heat other streams within the process and thereby reduce the heating costs in a process where a PSA unit is used. Nonetheless, heat integration was not investigated and therefore cryogenic distillation was chosen above the adsorption technique.

5.1.1. Validity adsorption model

The PSA column that is modeled in this study is compared to a dynamic model made by Sadeghzadeh Ahari et al. [70]. Sadeghzadeh Ahari modeled the pressurisation, adsorption, blow down and desorption of the column, but here only the adsorption steps are compared to each other.

The column dimensions and operating conditions are adjusted to match those of the study by Sadeghzadeh Ahari (L = 1 m and A_c = 0.00049 m^2). Subsequently, the nitrogen purity for different column lengths, adsorption times and inlet flow velocities is measured.

Figure 5.1 shows the dependency of the nitrogen purity on different parameters, compared to Sadeghzadeh Ahari. As can be seen in these figures, the models follow the same trend, but the model designed in this thesis approximates the nitrogen purity 1.5 mol% higher for the adsorption time dependency and around 1 mol% lower for the inlet flow velocity dependency. The difference between the data in Figure 5.1a is smaller. Also, for higher flow velocities and larger column lengths (as for the model designed in this research), the differences decrease.

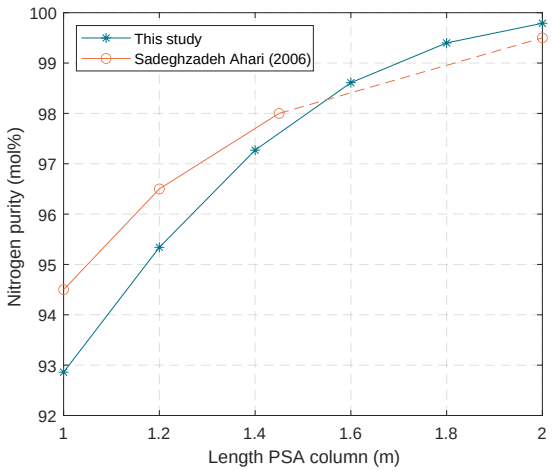

(a) For different column lengths.

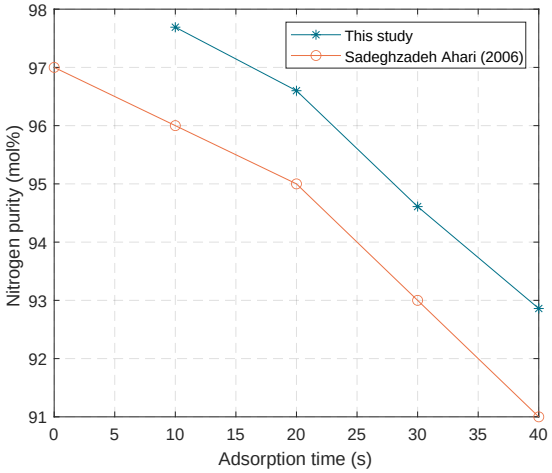

(b) For different adsorption cycle times.

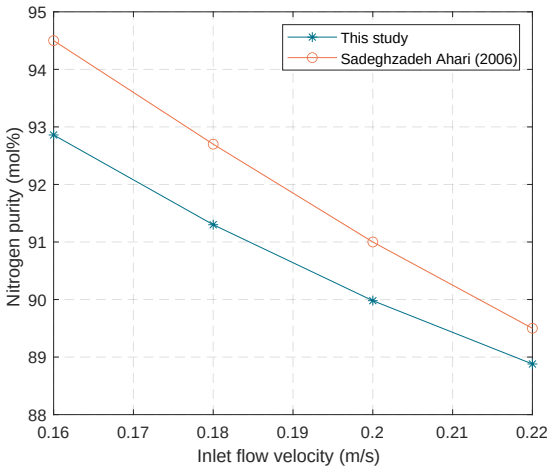

(c) For different inlet flow velocities.

Figure 5.1: Nitrogen purity dependency on different parameters, compared to Sadeghzadeh Ahari et al. (2006) [70].

5.2. Ammonia Separation

In a system with an AEL, a distillation column needs to be used for the separation of ammonia from the electrolyte since ammonia is dissolved in the electrolyte and a flash drum will be unable to provide sufficient separation. For an AEL based process, with an electrolyser that has a Faradaic efficiency of 70% and operates at a cell potential of 1.77 V, the energy consumption of the distillation unit represents 7.5% of the total energy consumption. Adsorbents and membranes have been proven to be able to separate ammonia from gaseous hydrogen and nitrogen, but separation of ammonia from an electrolyte has not been proven by this technique (see section 2.4).

For a system in which a PEMEL is used for the production of ammonia, flash separation is a feasible separation technique. Other separation technologies, such as distillation, PSA or membranes are unnecessarily more capital intensive than flash separation [72]. Especially for PEMEL cells that operate at higher pressures, such as 30 bar, a flash drum can be placed directly after the electrochemical cell, which saves pressurisation costs. For a PEMEL based process, with an electrolyser that has a Faradaic efficiency of 70% and operates at a cell potential of 1.77 V, the flash drum requires 4.9% of the total energy consumption of the process, which is 0.75 kWh $\cdot$ $kg_{NH_3}^{-1}$. This is higher than the 0.47 kWh $\cdot$ $kg_{NH_3}^{-1}$ that is required for the distillation of ammonia from hydrogen and nitrogen as found by Kugler et al. [40]. Kugler used a conversion rate of 35% and a Faradaic efficiency of 80% (in this study a 25% conversion and 70% Faradaic efficiency were assumed), which influences the concentration of ammonia in the

product stream and therefore the energy consumption of the separation step. An advantage of cells operating at a higher pressure and flashing at an intermediate pressure, is that this allows for easy storage of ammonia.

For both separation technologies, it was found that an ammonia concentration of at least 10 mol% is required for efficient separation. At concentrations below this value, the energy requirements for the separation process grow rapidly. This is the same result that Wang et al. found [91]. In order to reach this concentration of ammonia in the product streams, they recirculate the electrolyte until the required ammonia concentration is reached. For the separation of ammonia from an electrolyte, this observation can be attributed to the solubility of ammonia in a KOH solution [65]. For the separation of ammonia from a gaseous mixture of hydrogen and nitrogen, this observation is ascribed to the vapour pressure of ammonia, causing the presence of ammonia in the vapour phase [68].

5.3. Preferred electrochemical cell

In this thesis two processes are modeled, one for a process with an AEL and one for a process in which a PEMEL is used. The electrolyser choice influences the design of the entire process. Pre-treatment is influenced because the two electrolysers have different operating temperatures and pressures. While the separation steps are different due to a difference in components that are present in the product streams from the electrolysers. When comparing the two processes, all pre-treatment and separation steps in a PEMEL based process are less energy consuming. However, the final selection also depends on the energy consumption by the cell itself. Which type of electrochemical cell is best suited for ammonia synthesis and which type of cell requires the least amount of energy still needs to be proven.

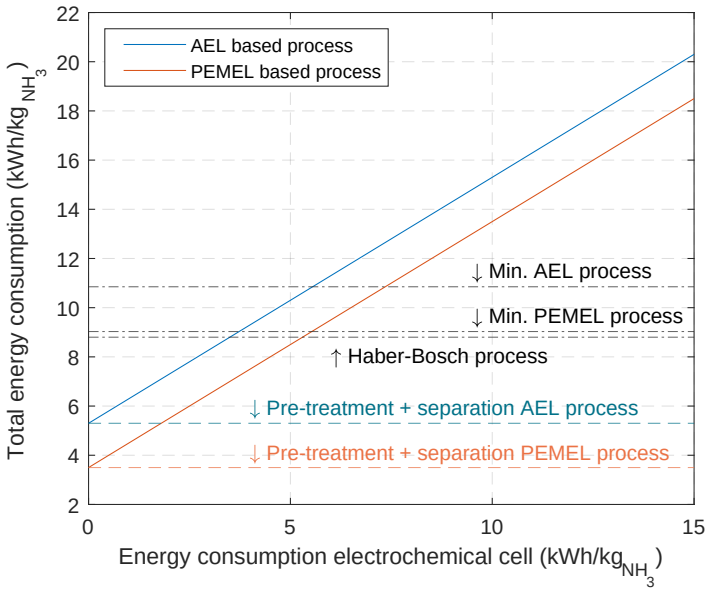

Figure 5.2: Total energy consumption of an AEL and a PEMEL based process compared.

Depending on the amount of energy required by the cell itself, the total energy consumption by the production process can be found in Figure 5.2. An AEL cell should always consume 1.80 kWh $\cdot$ $kg_{NH_3}^{-1}$ less energy than a PEMEL cell in order to be competitive with a PEMEL based process. This figure also shows the energy consumption of a Haber-Bosch process and the lower bounds for an AEL and a PEMEL process, which are based on a cell voltage of 1.17 V and a Faradaic efficiency of 100%. It can be observed that even in the most optimal situation, the electrochemical based processes require slightly more energy.

To illustrate the energy consumption by the different sub-process, a breakdown of the energy requirements for the different ammonia production routes is presented in Figure 5.3. For this illustration, a Faradaic efficiency of 70% and a cell potential of 1.77 V are assumed. It can be observed that for all electrochemical routes, the NH_3 electrolysis step is most energy intensive.

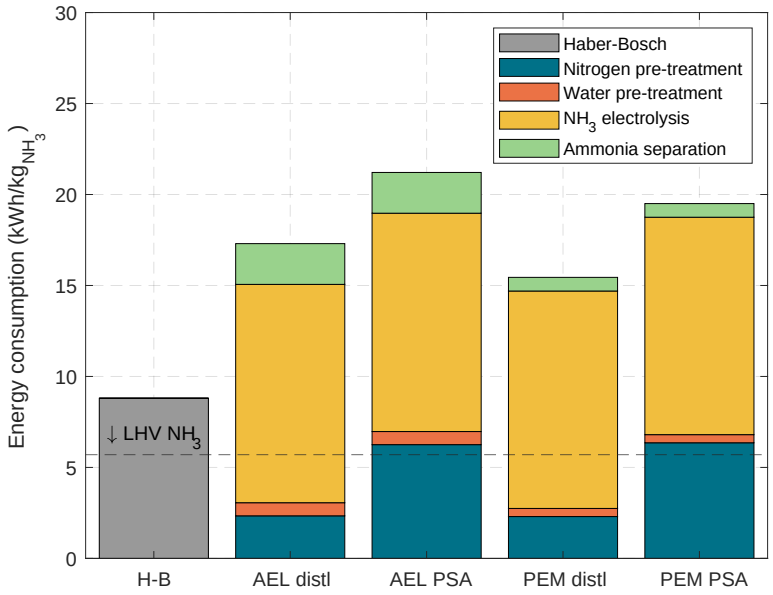

Figure 5.3: Energy requirements of the different sub-processes for different NH_3 production plants. For the electrochemical routes, a Faradaic efficiency of 70% and a cell potential of 1.77 V are assumed. Dashed horizontal line indicates the LHV of NH_3 (5.7 kWh $\cdot$ kg$^{-1}_{NH_3}$).

5.4. Required electrolyser operation parameters

In this section, the total energy consumption of an electrochemical ammonia synthesis process is compared to a Haber-Bosch based process with an energy consumption of 8.8 kWh $\cdot$ kg$^{-1}_{NH_3}$.

The pre-treatment and separation steps in an AEL based process require at least 5.30 kWh $\cdot$ kg$^{-1}_{NH_3}$. This means that the energy consumption of the electrochemical cell should be lower or equal to 3.50 kWh $\cdot$ kg$^{-1}_{NH_3}$. However, even with a Faradaic efficiency of 100% and at the standard equilibrium cell voltage of 1.17 V this is impossible. At these operating parameters, the electrochemical cell itself would require 5.55 kWh $\cdot$ kg$^{-1}_{NH_3}$.

The pre-treatment and separation steps require at least 3.50 kWh $\cdot$ kg$^{-1}_{NH_3}$ for a PEMEL cell based process. This results in the maximum allowed energy consumption by the PEMEL cell to be 5.30 kWh $\cdot$ kg$^{-1}_{NH_3}$. Also for this process, even in the most optimistic predictions for future ammonia electrolysers, with a Faradaic efficiency of 100% and at a cell potential of 1.17 V, the PEMEL cell requires 5.53 kWh $\cdot$ kg$^{-1}_{NH_3}$. This results in a total energy consumption of 9.66 kWh $\cdot$ kg$^{-1}_{NH_3}$. The target of being competitive with a Haber-Bosch process is not achieved with these operating parameters, but with optimisation of the process and the operating parameters (see chapter 7), this is perhaps possible. At a 70% Faradaic efficiency, the cell potential should be equal to or below 0.69 V to stay below the allowed energy consumption. However, this is below the standard equilibrium cell voltage, so no ammonia will be produced at this voltage.

The results for the electrochemical cell are compared to the results from a research by Wang et al. [91]. Wang estimated an energy consumption of the electrolyser of 11.82 kWh $\cdot$ kg$^{-1}_{NH_3}$, determined at an overpotential of 0.6 V (thus a cell potential of 1.77 V) and a Faradaic efficiency of 90%. Our results, 12.00 kWh $\cdot$ kg$^{-1}_{NH_3}$ for an AEL and 11.95 kWh $\cdot$ kg$^{-1}_{NH_3}$ for a PEMEL, come very close to these findings.

As discovered in this study, the energy requirements of an electrochemical process are well above the energy consumption of current Haber-Bosch based processes. However, electrolysers are not very efficient and optimised yet, while the Haber-Bosch process has been optimised for over a century. Therefore, this study represents one of the first process analyses of electrochemical ammonia production and allows for development in this area.

6

Conclusion

The focus of this thesis was to investigate different options for pre-treatment, electrochemical ammonia synthesis and separation steps, and to find the most optimal route for producing ammonia. Furthermore, technological performance targets for electrochemical ammonia synthesis were formulated.

Cryogenic distillation and pressure swing adsorption for nitrogen generation are modeled and compared in this study. It has been found that a distillation process has an energy consumption of 0.56 $kWh \cdot kg_{N_2}^{-1}$ and an adsorption process has an energy consumption of 1.82 $kWh \cdot kg_{N_2}^{-1}$. Based on the requirement that the process should consume the least amount of energy, a cryogenic distillation unit is preferred. Also when analysing the complete production processes with either a distillation or an adsorption step, the processes with a distillation unit demand the least amount of energy.

The ideal Faradaic efficiency of the cell lies above 70%, because at lower Faradaic efficiencies, the current that is required to achieve the pre-defined ammonia formation rate increases rapidly. An increase in cell potential is linearly related to an increase in energy consumption by the electrolyser and should therefore be minimised. A process where no electrolyte is needed would be the ideal process for ammonia production since the separation step of these processes is less energy consuming. Therefore, a PEMEL cell is considered the most promising type of electrochemical cell for an industrial ammonia synthesis process.

For an AEL based process, a distillation unit is required for the separation of ammonia from the electrolyte. This sub-process, including ammonia compression for storage, requires 2.24 $kWh \cdot kg_{NH_3}^{-1}$. For a PEMEL based process, flash separation has been proven to provide sufficient separation, with an energy requirement of 0.75 $kWh \cdot kg_{NH_3}^{-1}$.

The energy efficiency of the entire process is influenced by the applied cell potential and by the Faradaic efficiency for a fixed ammonia formation rate. Only at a 100% Faradaic efficiency and a cell potential below 1.3 V, an overall energy efficiency of above 50% can be achieved. Not for an alkaline cell, nor for a PEMEL cell based process it is possible to stay below the energy consumption of a Haber-Bosch process. However, at Faradaic efficiencies of 100% and zero overtotential, a PEMEL cell based process does come close with a total energy consumption of 9.66 $kWh \cdot kg_{NH_3}^{-1}$.

To conclude, an AEL or a PEMEL based ammonia synthesis process should be able to produce ammonia at an energy consumption of around 8.8 $kWh \cdot kg_{NH_3}^{-1}$. In order to achieve this, low energy consuming pre-treatment and separation technologies are selected. With a Faradaic efficiency of 70%, cell potential of 1.77 V, nitrogen conversion rate of 25 mol% and an ammonia concentration of 10 mol% in the electrolyser product stream, the energy consumptions for AEL and PEMEL based processes are, respectively, 12.00 $kWh \cdot kg_{NH_3}^{-1}$ and 11.95 $kWh \cdot kg_{NH_3}^{-1}$.

7

Recommendations

7.1. Adsorption model

In this thesis, only the adsorption step of the PSA was modeled. In order to get more accurate results it is advised to also take into account the pressurisation, blow down and desorption steps since these steps require energy as well.

The dimensions of the adsorption column were set equal to those modeled by Sanchez et al. [72]. This resulted in a low throughput per column and therefore a large number of parallel operating columns was needed, which might be not economic. In further modeling of the PSA unit, its dimensions should be scaled up and its validity should be checked.

At high pressures, which are needed for a 99.9 mol% nitrogen purity, the nitrogen recovery is relatively low. This recovery rate should be increased to make PSA a reasonable alternative to cryogenic distillation for air separation. Better oxygen adsorbents could be researched or a different adsorber set up could be tried. It is also possible that ammonia synthesis with PSA for nitrogen generation is only interesting at low production capacities.

7.2. Separation technologies

The energy consumption of the modeled distillation and flash separation processes strongly depend on the ammonia concentration of the cell's product stream. Therefore, options to increase the ammonia concentration, such as product recycles into the electrolyser, longer residence times or different temperatures and pressures, should be explored.

For the flash separation of ammonia from the gaseous product stream from a PEMEL cell, it was assumed that only hydrogen and nitrogen were present besides ammonia due to the zero cross-over assumption. In further studies it should be checked whether this assumption is valid, because it is possible that at higher pressures cross-over of small particles does take place.

7.3. Electrolyser analysis

In this study, Faraday's law was used to calculate the required current for the production of a fixed amount of ammonia, and the cell's power is calculated as the sum of the cell potential and the total current. These calculations assume a known Faradaic efficiency and current or give an indication for what these values should be. However, this does not give an indication of the process inside the electrochemical cell. For our calculations this is not required, but for further research it is valuable to also take into account the influence of the operating parameters (temperature, pressure, volume flows, etc.) on overpotentials, the ammonia formation rate and Faradaic efficiencies. Moreover, it is valuable to analyse the effect of the cell potential on the ammonia formation rate, to determine the most optimum operating potential. An electrical energy efficiency of 100% was assumed in this study. However, in

future studies, this efficiency should be investigated, since it is expected that there are losses due to, for example, heat production inside the cell. For a better understanding of the cell's operation, reactions inside the cell, heat and mass transfer and flow patterns will need to be taken into account. Also, other types of electrochemical cells, such as SOELs and AEMELs should be further researched in order to determine which cell is best fit for an ammonia production process.

7.4. Overall recommendations

Generally, the process should be optimised to increase energy efficiencies. This study has indicated what technologies are likely feasible and what technologies or process units have significant energy requirements. Heat integration plays an important role in the optimisation of the process, but also stream recycles and a different set up for the PSA columns could increase the system's efficiency.

It is advised to compare the different technologies and different overall processes on other criteria than the energy consumption. An exergy balance will give more insight into where useful energy is lost and a cost analysis will give better insights in the capital and operating costs. Additionally, the environmental impact, such as CO_2 emissions, of the different technologies should be compared.

Appendices

A

Stoichiometric carbon dioxide emissions Haber-Bosch process

The stoichiometric CO_2 emissions of the Haber-Bosch ammonia synthesis process are based on the following assumptions:

- 60 mol% methane reacts in the first SMR reactor and 39 mol% methane reacts in the second SMR reactor [9].
- All carbon monoxide is converted in the WGSR.
- All hydrogen converts to ammonia.

Table A.1: Stoichiometric CO_2 emissions Haber-Bosch process

	Reaction	CH_4 (mol)	CO (mol)	CO_2 (mol)	H_2 (mol)	NH_3 (mol)
SMR	$CH_4 + H_2O \rightarrow CO + 3H_2$	0.6	0.6	-	1.8	-
	$2CH_4 + O_2 \rightarrow 2CO + 4H_2$	0.39	0.39	-	0.78	-
WGSR	$CO + H_2O \rightarrow CO_2 + H_2$	-	0.99	0.99	0.99	-
Ammonia synthesis	$N_2 + 3H_2 \rightarrow 2NH_3$	-	-	-	3.57	2.38

With molar masses $M_{CO_2} = 44.01\ g \cdot mol^{-1}$ and $M_{NH_3} = 17.031\ g \cdot mol^{-1}$:

CO_2 emissions: $\frac{M_{CO_2} \cdot mol_{CO_2}}{M_{NH_3} \cdot mol_{NH_3}} = 1.07\ kg_{CO_2} \cdot kg_{NH_3}^{-1}$

B

Gibbs free energy for nitrogen reduction

The overall reaction for nitrogen reduction with water is shown in Equation B.1 and some thermochemical properties for the elements are given in Table B.1.

$$\frac{1}{2}N_2 + \frac{3}{2}H_2O \rightarrow \frac{3}{4}O_2 + NH_3 \tag{B.1}$$

Table B.1: Thermochemical properties of components for ammonia formation at 298 K and 1 atm

	N_2	H_2O	O_2	NH_3
Enthalpy of formation, h_f^0 (kJ · mol^{-1})	0	-285.83	0	-46.19
Absolute entropy, s^0 (J · mol^{-1}K^{-1})	191.5	69.95	205.03	192.33

The Gibbs free energy of formation, ΔG^0, is found as follows:

$$\Delta G^0 = \Delta H^0 - T\Delta S^0 \tag{B.2}$$

$\Delta H^0 = -\frac{1}{2}h^0_{N_2} - \frac{3}{2}h^0_{H_2O} + \frac{3}{4}h^0_{O_2} + h^0_{NH_3}$ = 382.55 kJ

$\Delta S^0 = -\frac{1}{2}s^0_{N_2} - \frac{3}{2}s^0_{H_2O} + \frac{3}{4}s^0_{O_2} + s^0_{NH_3}$ = 145.43 J · K^{-1}

Subsequently, the Gibbs free energy of formation at 298 K and 1 atm can be found:

$\Delta G^0 = \Delta H^0 - T\Delta S^0$ = 339 kJ · mol$^{-1}_{NH_3}$ = 5.54 kWh · kg$^{-1}_{NH_3}$.

C

Discretisation PSA column

The adsorption column for air separation is discretised over its length into space steps with length Δz and over time with time steps of Δt using the Euler backward method for first derivatives and a central difference scheme for second derivatives. An illustration of the discretisation in time and space of the column is shown in Figure C.1.

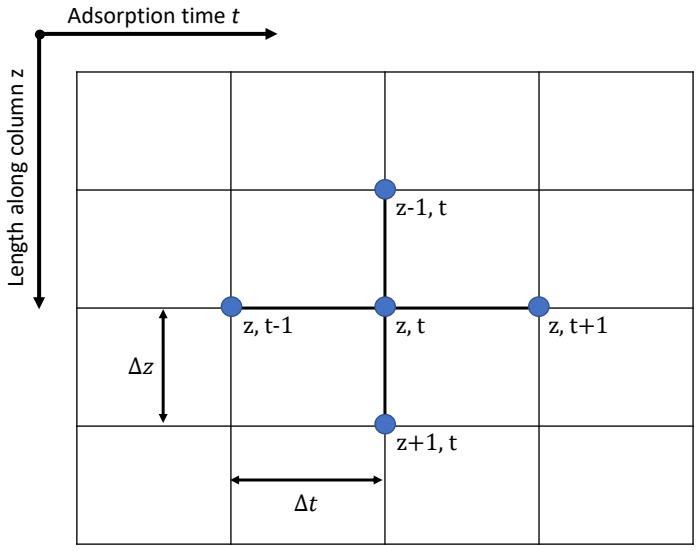

Figure C.1: Illustration of the discretisation in time and space of the PSA column.

With L_t as the length of one time step t and L_i as the length of one step along the length of the adsorption column, the terms in Equation 3.1 are discretised as follows:

$$\frac{\delta C_i}{\delta t} = \frac{C_i(i,t) - C_i(z,t-1)}{L_t} \tag{C.1}$$

$$\frac{\delta^2 C_i}{\delta z^2} = \frac{C_i(z,t) - 2C_i(z-1,t) + C_i(z-2,t)}{L_i^2} \tag{C.2}$$

$$\frac{\delta C_i}{\delta z} = \frac{C_i(z,t) - C_i(z-1,t)}{L_i} \tag{C.3}$$

An expression for the change in flow velocity along the length of the column can be found by rewriting Equation 3.2 and results in:

$$\frac{\delta v}{\delta z}(z,t) = -\frac{1-\epsilon}{\epsilon C_{tot}(z,t)} \sum_i \frac{\delta q_i}{\delta t}(z,t) \tag{C.4}$$

$$\frac{\delta q_i}{\delta t} = \frac{q_i(z,t) - q_i(z,t-1)}{L_t} \tag{C.5}$$

Where:

$$q_i(z,t) = \frac{L_t k_i q_i^*(z,t) + q_i(z,t-1)}{1 + L_t k_i} \tag{C.6}$$

Since:

$$k_i(q_i^*(z,t) - q_i(z,t)) = \frac{q_i(z,t) - q_i(z,t-1)}{L_t} \tag{C.7}$$

Which can be found by combining Equation 3.3 and Equation C.5.

D

Separation process of ammonia from an AEL solute product stream

Table D.1 gives the distillation column specification and energy requirement for a separation unit that separates ammonia from a 1 M KOH solution originating from an AEL.

Table D.1: Distillation column specifications and energy requirement for a separation process of ammonia from a 1 M KOH solution for different concentrations of ammonia in the solute product stream.

Concentration ammonia (mol%)	Number of stages (-)	Feed stage (-)	Reflux ratio (-)	Distillate to feed ratio (-)	Ammonia recovery (mol%)	Energy consumption ($kWh \cdot kg_{NH_3}^{-1}$)
4	32	7	1.7	0.0392	99.4	10.04
5	25	4	1.5	0.0491	99.9	8.13
10	22	4	1.3	0.0995	99.5	1.75
15	14	4	1.25	0.147	99.5	1.36
20	10	5	1.15	0.1959	99.4	1.11

E

Stream summary

E.1. AEL with distillation

	AIR1	AIR2	AMM1	AMM2	AMM3	AMMONIA
Temperature (K)	569.45	89.95	239.45	240.15	466.85	298.15
Pressure (bar)	6	6	1	1	10	10
Vapor Frac	1	0	0	1	1	0
Solid Frac			0	0	0	0
Mole Flow (kmol/hr)	10683.43	10683.43	3670.06	3670.06	3670.06	3670.06
Mass Flow (kg/hr)	308646.97	308646.97	62503.14	62503.14	62503.14	62503.14
Volume Flow (cum/hr)	84460.31	377.41	91.37	72334.18	13959.05	103.76
Enthalpy (Gcal/hr)	20.50	-29.81	-62.36	-41.91	-34.62	-57.89
Mole Flow (kmol/hr)						
HYDRO-01						
NITRO-01	8333.08	8333.08				
OXYGE-01	2350.36	2350.36				
AMMON-01			3670.06	3670.06	3670.06	3670.06
WATER						
K+						
OH-						
NH4+						
KOH(S)						

	BOTTOM	DRY-AIR	GASES	KOH	KOH-SOL
Temperature (K)	373.65	298.15	353.15	298.15	298.15
Pressure (bar)	1	1	1	1	1
Vapor Frac	0	1	0	0	0
Solid Frac	0		1	1	0
Mole Flow (kmol/hr)	33214.94	10683.43	11956.95	716.80	41099.80
Mass Flow (kg/hr)	612723.43	308646.97	289075.67	40216.40	754814.11
Volume Flow (cum/hr)	604.22	264690.52			750.23
Enthalpy (Gcal/hr)	-2210.21	-0.02	0	0	-2740.99
Mole Flow (kmol/hr)					
HYDRO-01			2371.00		
NITRO-01		8333.08	5631.41		
OXYGE-01		2350.36	3954.55		
AMMON-01	18.44				
WATER	31765.36				39666.20
K+	716.80				716.80
OH-	716.80				716.80
NH4+	< 0.001				
KOH(S)				716.80	

	NIT1	NIT2	OXYGEN	SOLUTE	WAT1	WATER
Temperature (K)	77.35	353.15	84.25	353.15	353.15	298.15
Pressure (bar)	1	1	1	1	1	1
Vapor Frac	0	1	0	0.122	0	0
Solid Frac				0	0	0
Mole Flow (kmol/hr)	7478.40	7478.40	3205.03	36885.00	41099.80	39666.20
Mass Flow (kg/hr)	209507.54	209507.54	99139.42	675226.57	754814.16	714597.70
Volume Flow (cum/hr)	260.39	219575.72	94.84	131779.1	740.95	716.63
Enthalpy (Gcal/hr)	-21.58	2.85	-9.77	-2247.52	-2753.58	-2709.65
Mole Flow (kmol/hr)						
HYDRO-01						
NITRO-01	7475.51	7475.51	857.56			
OXYGE-01	2.89	2.89	2347.47			
AMMON-01				3688.49		
WATER				31765.35	39666.20	39666.20
K+				716.80	716.80	
OH-				716.80	716.80	
NH4+				0.01		
KOH(S)						

E.2. AEL with PSA

Table E.1: Stream summary for an AEL with distillation process

	ABS1	ABSORBED	AIR1	AIR2	AIR3	AMM1
Temperature (K)	298.15	298.15	658.65	298.15	298.15	239.45
Pressure (bar)	9.4	9.4	9.4	9.4	9.4	1
Vapor Frac	0	0	1	1	1	0
Solid Frac	0	0	0	0	0	0
Mole Flow (kmol/hr)	319.36	55888.68	63525.90	63525.90	362.10	3670.06
Mass Flow (kg/hr)	9263.79	1621160	1835280	1835280	10461.09	62503.19
Volume Flow (cum/hr)			371201.08	166721.26	950.31	91.37
Enthalpy (Gcal/hr)	0	0	163.46	-1.14	-0.01	-62.36
Mole Flow (kmol/hr)						
HYDRO-01						
NITRO-01	239.75	41955.86	49550.20	49550.20	282.44	
OXYGE-01	79.62	13932.82	13975.70	13975.70	79.66	
AMMON-01						3670.06
WATER						
K+						
OH-						
NH4+						
KOH(S)						

	AMM2	AMM3	AMMONIA	BOTTOM	DRY-AIR
Temperature (K)	240.15	466.85	298.15	373.65	298.15
Pressure (bar)	1	10	10	1	1
Vapor Frac	1	1	0	0	1
Solid Frac	0	0	0	0	0
Mole Flow (kmol/hr)	3670.06	3670.06	3670.06	33214.94	63525.9
Mass Flow (kg/hr)	62503.19	62503.19	62503.19	612723.38	1835280.00
Volume Flow (cum/hr)	72334.23	13959.06	103.76	604.22	1573910.00
Enthalpy (Gcal/hr)	-41.91	-34.62	-57.89	-2210.21	-0.12
Mole Flow (kmol/hr)					
HYDRO-01					
NITRO-01					49550.20
OXYGE-01					13975.70
AMMON-01	3670.06	3670.06	3670.06	18.439	
WATER				31765.36	
K+				716.80	
OH-				716.80	
NH4+				< 0.001	
KOH(S)					

	GASES	KOH	KOH-SOL	NIT1	NIT2	NIT3
Temperature (K)	353.15	298.15	298.15	298.15	298.15	298.15
Pressure (bar)	1	1	1	9.4	9.4	9.4
Vapor Frac	0	0	0	0	0	1
Solid Frac	1	1	0	0	0	0
Mole Flow (kmol/hr)	11956.95	716.80	41099.80	42.73	7478.41	7478.41
Mass Flow (kg/hr)	289095.76	40216.41	754814.14	1197.30	209527.82	209527.82
Volume Flow (cum/hr)			750.23			19647.98
Enthalpy (Gcal/hr)	0		-2740.98	0	0	-0.13
Mole Flow (kmol/hr)						
HYDRO-01	2371.00					
NITRO-01	5626.36			42.69	7470.47	7470.47
OXYGE-01	3959.58			0.05	7.94	7.94
AMMON-01						
WATER						
K+			716.80			
OH-			716.80			
NH4+						
KOH(S)		716.80				

	NIT4	NIT5	SOLUTE	WAT1	WATER
Temperature (K)	195.55	353.15	353.15	353.15	298.15
Pressure (bar)	1	1	1	1	1
Vapor Frac	1	1	0.122	0	0
Solid Frac	0	0	0	0	0
Mole Flow (kmol/hr)	7478.41	7478.41	36885.00	41099.80	39666.20
Mass Flow (kg/hr)	209527.82	209527.82	675226.57	754814.16	714597.73
Volume Flow (cum/hr)	121247.56	219575.81	131779.21	740.95	716.63
Enthalpy (Gcal/hr)	-5.36	2.85	-2247.52	-2753.58	-2709.65
Mole Flow (kmol/hr)					
HYDRO-01					
NITRO-01	7470.47	7470.47			
OXYGE-01	7.94	7.94			
AMMON-01			3688.49		
WATER			31765.35	39666.20	39666.20
K+			716.80	716.80	
OH-			716.80	716.80	
NH4+			0.01		
KOH(S)					

E.3. PEM with distillation

Table E.2: Stream summary for a PEMEL with distillation process

	AIR1	AIR2	AMMONIA	ANODE	CATHODE
Temperature (K)	569.45	90.15	172.95	353.15	353.15
Pressure bar	6	6	15	30	30
Vapor Frac	1	0	0	0	0
Mole Flow kmol/hr	10496.00	10496.00	3670.05	18098.74	11543.93
Mass Flow kg/hr	303232.07	303232.07	62503.51	381148.27	221614.16
Volume Flow cum/hr	82978.53	371.14	82.02		
Enthalpy Gcal/hr	20.14	-29.26	-67.17	0.00	0.00
Mole Flow kmol/hr					
HYDRO-01			0.08		2362.27
NITRO-01	8186.88	8186.88	0.15		5507.03
OXYGE-01	2309.12	2309.12		3939.96	
AMMON-01			3669.83		3674.64
WATER				14158.78	

	DRY-AIR	GASES	NIT1	NIT2	NIT3	NIT4
Temperature (K)	298.15	172.95	77.35	123.15	231.35	353.15
Pressure bar	1	15	1	6	30	30
Vapor Frac	1	1	0	1	1	1
Mole Flow kmol/hr	10496.00	7873.88	7347.20	7347.20	7347.20	7347.20
Mass Flow kg/hr	303232.07	159110.65	205831.99	205831.99	205831.99	205831.99
Volume Flow cum/hr	260046.79	7302.24	255.82	11604.69	4511.83	7197.98
Enthalpy Gcal/hr	-0.02	-7.19	-21.21	-9.31	-4.05	2.56
Mole Flow kmol/hr						
HYDRO-01		2362.19				
NITRO-01	8186.88	5506.88	7344.35	7344.35	7344.35	7344.35
OXYGE-01	2309.12		2.85	2.85	2.85	2.85
AMMON-01		4.80				
WATER						

	OXYGEN1	OXYGEN2	WAT-REC	WAT1	WAT2	WATER
Temperature (K)	84.25	298.15	298.15	298.35	353.15	298.15
Pressure bar	1	1	1	30	30	1.
Vapor Frac	0	1	0	0	0.	0
Mole Flow kmol/hr	3148.80	4045.65	14053.09	22033.00	22033.00	22033.00
Mass Flow kg/hr	97400.06	127977.39	253170.88	396930.66	396930.66	396930.66
Volume Flow cum/hr	93.18	100176.09	254.71	399.42	422.63	399.34
Enthalpy Gcal/hr	-9.60	-6.12	-965.81	-1513.90	-1490.36	-1514.24
Mole Flow kmol/hr						
HYDRO-01						
NITRO-01	842.53					
OXYGE-01	2306.27	3939.92	0.04			
AMMON-01						
WATER		105.72	14053.06	22033.00	22033.00	22033.00

E.4. PEM with PSA

Table E.3: Stream summary for a PEMEL with PSA process

	ADS1	ADSORBED	AIR1	AIR2	AIR3
Temperature C	0.05	0.05	658.65	298.15	298.15
Pressure bar	9.4	9.4	9.4	9.4	9.4
Vapor Frac	0	0	1	1	1
Mole Flow kmol/hr	319.02	55827.78	63400.00	63400.00	361.38
Mass Flow kg/hr	9253.42	1619350.00	1831640.00	1831640.00	10440.36
Volume Flow cum/hr			370465.41	166390.84	948.43
Enthalpy Gcal/hr	-0.01	-1.00	163.14	-1.13	-0.01
Mole Flow kmol/hr					
HYDRO-01					
NITRO-01	239.56	41922.42	49452.00	49452.00	281.88
OXYGE-01	79.46	13905.36	13948.00	13948.00	79.50
AMMON-01					
WATER					

	AMMONIA	ANODE	CATHODE	DRY-AIR	GASES
Temperature C	172.95	353.15	353.15	298.15	172.95
Pressure bar	15	30	30	1	15
Vapor Frac	0	0	0	1	1
Mole Flow kmol/hr	3670.02	18116.66	11605.53	63400.00	7935.52
Mass Flow kg/hr	62502.86	381540.06	223339.85	1831640.00	160836.99
Volume Flow cum/hr	82.02			1570790.00	7357.76
Enthalpy Gcal/hr	-67.16	0	0	-0.12	-7.25
Mole Flow kmol/hr					
HYDRO-01	0.08		2362.27		2362.19
NITRO-01	0.15		5568.63	49452	5568.48
OXYGE-01		3944.88		13948	
AMMON-01	3669.79		3674.64		4.84
WATER		14171.78			

	NIT1	NIT2	NIT3	NIT4	NIT5
Temperature C	0.05	0.05	293.15	452.55	353.15
Pressure bar	9.4	9.4	9.4	30	30
Vapor Frac	0	0	1	1	1
Mole Flow kmol/hr	42.36	7413.72	7413.72	7413.72	7413.72
Mass Flow kg/hr	1186.94	207715.04	207715.04	207715.04	207715.04
Volume Flow cum/hr			19142.00	9377.82	7263.09
Enthalpy Gcal/hr	-0.001	-0.130	-0.39	7.87	2.58
Mole Flow kmol/hr					
HYDRO-01					
NITRO-01	42.32	7405.95	7405.95	7405.95	7405.95
OXYGE-01	0.04	7.77	7.77	7.77	7.77
AMMON-01					
WATER					

	OXYGEN	WAT-REC	WAT1	WAT2	WATER
Temperature C	353.15	353.15	298.35	353.15	298.15
Pressure bar	30	30	30	30	1
Vapor Frac	1	0	0	0	0
Mole Flow kmol/hr	4009.87	14106.79	22046.00	22046.00	22046.00
Mass Flow kg/hr	127354.87	254185.20	397164.86	397164.86	397164.86
Volume Flow cum/hr	3872.23	270.65	399.65	422.88	399.58
Enthalpy Gcal/hr	-2.60	-953.97	-1514.79	-1491.24	-1515.13
Mole Flow kmol/hr					
HYDRO-01					
NITRO-01					
OXYGE-01	3941.49	3.39			
AMMON-01					
WATER	68.39	14103.39	22046.00	22046.00	22046.00

Bibliography

[1] E. Afshari, S. Khodabakhsh, N. Jahantigh, and S. Toghyani. Performance assessment of gas crossover phenomenon and water transport mechanism in high pressure PEM electrolyzer. *International Journal of Hydrogen Energy*, 11 2020. ISSN 03603199. doi: 10.1016/j.ijhydene.2020.10.180.

[2] Air Products and Chemicals. PRISM ® Nitrogen Series Membrane Generators. Technical report, 2006.

[3] Air Products and Chemicals. PRISM ® PSA Nitrogen Generation System. Technical report, 2017.

[4] Ibrahim A. Amar, Rong Lan, Christophe T.G. Petit, Valeria Arrighi, and Shanwen Tao. Electrochemical synthesis of ammonia based on a carbonate-oxide composite electrolyte. *Solid State Ionics*, 182(1):133–138, 2011. ISSN 01672738. doi: 10.1016/j.ssi.2010.11.009. URL http://dx.doi.org/10.1016/j.ssi.2010.11.009.

[5] Ibrahim A. Amar, Rong Lan, Christophe T.G. Petit, and Shanwen Tao. Solid-state electrochemical synthesis of ammonia: A review. *Journal of Solid State Electrochemistry*, 15(9):1845–1860, 2011. ISSN 14328488. doi: 10.1007/s10008-011-1376-x.

[6] Márcia Andrade, Sandra C. Rodrigues, and Adélio Mendes. High performing CMS adsorbent for O2 / N2 separation. *Microporous and Mesoporous Materials*, 296:109989, 4 2020. ISSN 13871811. doi: 10.1016/j.micromeso.2019.109989. URL https://linkinghub.elsevier.com/retrieve/pii/S1387181119308480.

[7] Mathew Aneke and Meihong Wang. Potential for improving the energy efficiency of cryogenic air separation unit (ASU) using binary heat recovery cycles. *Applied Thermal Engineering*, 81:223–231, 4 2015. ISSN 13594311. doi: 10.1016/j.applthermaleng.2015.02.034.

[8] Max Appl. Ullmann Encyclopedia for industrial chemistry - Ammonia. 2006.

[9] M Batool and W Wetzels. Decarbonisation Options for the Dutch Fertiliser Industry. Technical report, PBL Netherlands Environmental Assessment Agency, 2019. URL www.pbl.nl/en.

[10] Dmitri Bessarabov and Pierre Millet. *The PEM Water Electrolysis Plant*. 2018. ISBN 9780081028308. doi: 10.1016/b978-0-08-102830-8.00001-1.

[11] Alexander Buttler and Hartmut Spliethoff. Current status of water electrolysis for energy storage, grid balancing and sector coupling via power-to-gas and power-to-liquids: A review. *Renewable and Sustainable Energy Reviews*, 82(February 2017):2440–2454, 2018. ISSN 18790690. doi: 10.1016/j.rser.2017.09.003.

[12] Carl Linde. Process of Producing Low Temperatures, the Liquefaction of Gases, and the Separation of the Constituents of Gaseous Mixtures, 7 1895.

[13] Cheng Chen and Guilin Ma. Proton conduction in BaCe1-xGdxO3-α at intermediate temperature and its application to synthesis of ammonia at atmospheric pressure. *Journal of Alloys and Compounds*, 485(1-2):69–72, 2009. ISSN 09258388. doi: 10.1016/j.jallcom.2009.05.108.

[14] Shiming Chen, Siglinda Perathoner, Claudio Ampelli, Chalachew Mebrahtu, Dangsheng Su, and Gabriele Centi. Electrocatalytic Synthesis of Ammonia at Room Temperature and Atmospheric Pressure from Water and Nitrogen on a Carbon-Nanotube-Based Electrocatalyst. *Angewandte Chemie - International Edition*, 56(10):2699–2703, 2017. ISSN 15213773. doi: 10.1002/anie.201609533.

[15] Shiming Chen, Siglinda Perathoner, Claudio Ampelli, Chalachew Mebrahtu, Dangsheng Su, and Gabriele Centi. Electrocatalytic Synthesis of Ammonia at Room Temperature and Atmospheric Pressure from Water and Nitrogen on a Carbon-Nanotube-Based Electrocatalyst. *Angewandte Chemie International Edition*, 56(10):2699–2703, 3 2017. ISSN 14337851. doi: 10.1002/anie.201609533. URL http://doi.wiley.com/10.1002/anie.201609533.

[16] Baochen Cui, Zhongjun Yu, Shuzhi Liu, Jianhua Zhang, Xianjun Liu, Chang Liu, and Zhihua Zhang. Highly selective and efficient ammonia synthesis from N2 and H2O via an iron-based electrolytic-chemical cycle. *International Journal of Hydrogen Energy*, 45(1):94–102, 1 2020. ISSN 03603199. doi: 10.1016/j.ijhydene.2019.10.144.

[17] Ibrahim Dincer and Marc A. Rosen. Exergy Analysis of Fuel Cell Systems. In *Exergy*, pages 363–382. Elsevier, 1 2013. doi: 10.1016/b978-0-08-097089-9.00018-8.

[18] Engie. ENGIE-YARA Renewable Hydrogen and Ammonia Deployment in Pilbara YURI Phase 0: Feasibility Study Public Report. Technical report, 10 2020.

[19] Engineers Edge. Viscosity of Air, Dynamic and Kinematic. URL https://www.engineersedge.com/physics/viscosity_of_air_dynamic_and_kinematic_14483.htm.

[20] European Commission. Large Volume Inorganic Chemicals - Ammonia, Acids and Fertilisers. Technical report, 2007. URL https://eippcb.jrc.ec.europa.eu/reference/large-volume-inorganic-chemicals-ammonia-acids-and-fertilisers.

[21] Carlos A. Fernandez, Nicholas M. Hortance, Yu Hsuan Liu, Jeonghoon Lim, Kelsey B. Hatzell, and Marta C. Hatzell. Opportunities for intermediate temperature renewable ammonia electrosynthesis. *Journal of Materials Chemistry A*, 8(31):15591–15606, 2020. ISSN 20507496. doi: 10.1039/d0ta03753b.

[22] Food and Agriculture Organization. World fertilizer trends and outlook to 2020. 2017.

[23] Thomas F. Fuller and John N. Harb. Industrial Electrolysis, Electrochemical Reactors, and Redox-Flow Batteries. In *Electrochemical Engineering*, chapter 14. John Wiley & Sons, 2018. ISBN 9788578110796. URL http://dx.doi.org/10.1016/j.tws.2012.02.007.

[24] Thomas F. Fuller and John N. Harb. Fuel-Cell Fundamentals. In *Electrochemical Engineering*, chapter 9. John Wiley & Sons, 2018.

[25] Ioannis Garagounis, Vasileios Kyriakou, Aglaia Skodra, Eirini Vasileiou, and Michael Stoukides. Electrochemical Synthesis of Ammonia in Solid Electrolyte Cells. *Frontiers in Energy Research*, 2:1, 1 2014. ISSN 2296-598X. doi: 10.3389/fenrg.2014.00001. URL http://journal.frontiersin.org/article/10.3389/fenrg.2014.00001/abstract.

[26] P J Gellings and H J M Bouwmeester. *The CRC Handbook of Solid State Electrochemistry Library of Congr ess Cataloging-in-Publication Data*. CRC Press, 1997. ISBN 0849389569.

[27] Ming Geng and Zhenhao Duan. Prediction of oxygen solubility in pure water and brines up to high temperatures and pressures. *Geochimica et Cosmochimica Acta*, 74(19):5631–5640, 10 2010. ISSN 00167037. doi: 10.1016/j.gca.2010.06.034.

[28] S. Giddey, S. P.S. Badwal, and A. Kulkarni. Review of electrochemical ammonia production technologies and materials. *International Journal of Hydrogen Energy*, 38(34):14576–14594, 11 2013. ISSN 03603199. doi: 10.1016/j.ijhydene.2013.09.054.

[29] Jamie R. Gomez, John Baca, and Fernando Garzon. Techno-economic analysis and life cycle assessment for electrochemical ammonia production using proton conducting membrane. *International Journal of Hydrogen Energy*, 45(1):721–737, 2020. ISSN 03603199. doi: 10.1016/j.ijhydene.2019.10.174. URL https://doi.org/10.1016/j.ijhydene.2019.10.174.

[30] Grigorii Soloveichik. Renewable Energy to Fuels Through Utilization of EnergyDense Liquids (REFUEL) Program Overview. Technical report, ARPA-E, 2016. URL https://arpa-e.energy.gov/technologies/programs/refuel.

[31] S. M. Haile, G. Staneff, and K. H. Ryu. Non-stoichiometry, grain boundary transport and chemical stability of proton conducting perovskites. *Journal of Materials Science*, 36(5):1149–1160, 2001. ISSN 00222461. doi: 10.1023/A:1004877708871.

[32] Heinz-Wolfgang Häring. The Air Gases Nitrogen, Oxygen and Argon. In *Industrial Gases Processing*, chapter 2, pages 9–109. John Wiley & Sons, Weinheim, Germany, 2008. doi: 10.1002/9783527621248.ch2. URL http://doi.wiley.com/10.1002/9783527621248.ch2.

[33] Institute for Sustainable Process Technology. Power to Ammonia | Feasibility study for the value chains and business cases to produce CO2-free ammonia suitable for various market applications. Technical report, 2017.

[34] H. Ishaq and I. Dincer. Analysis and optimization for energy, cost and carbon emission of a solar driven steam-autothermal hybrid methane reforming for hydrogen, ammonia and power production. *Journal of Cleaner Production*, 234:242–257, 10 2019. ISSN 09596526. doi: 10.1016/j.jclepro.2019.06.027.

[35] Jeong Geun Jee, Min Bae Kim, and Chang Ha Lee. Pressure swing adsorption processes to purify oxygen using a carbon molecular sieve. *Chemical Engineering Science*, 60(3):869–882, 2005. ISSN 00092509. doi: 10.1016/j.ces.2004.09.050.

[36] Robert Kender, Bernd Wunderlich, Ingo Thomas, Andreas Peschel, Sebastian Rehfeldt, and Harald Klein. Pressure-driven dynamic simulation of start up and shutdown procedures of distillation columns in air separation units. *Chemical Engineering Research and Design*, 147:98–112, 7 2019. ISSN 02638762. doi: 10.1016/j.cherd.2019.04.031.

[37] A Keys, M Van Hout, and B Daniëls. Decarbonisation options for the Dutch steel industry. Technical report, TNO - ECN, 2019. URL www.pbl.nl/en.

[38] Masaaki Kitano, Yasunori Inoue, Masato Sasase, Kazuhisa Kishida, Yasukazu Kobayashi, Kohei Nishiyama, Tomofumi Tada, Shigeki Kawamura, Toshiharu Yokoyama, Michikazu Hara, and Hideo Hosono. Self-organized Ruthenium-Barium Core-Shell Nanoparticles on a Mesoporous Calcium Amide Matrix for Efficient Low-Temperature Ammonia Synthesis. *Angewandte Chemie International Edition*, 57(10):2648–2652, 3 2018. ISSN 14337851. doi: 10.1002/anie.201712398. URL http://doi.wiley.com/10.1002/anie.201712398.

[39] K. A. Kondrashina, A. A. Kozlova, A. N. Petukhov, D. N. Shablikin, M. M. Trubyanov, and I. V. Vorotyntsev. Thermodynamic modelling of VLE behaviour at the high purification of R717 refrigerant by high-pressure batch distillation. *Journal of Physics: Conference Series*, 1134(1), 2018. ISSN 17426596. doi: 10.1088/1742-6596/1134/1/012060.

[40] K. Kugler, B. Ohs, M. Scholz, and M. Wessling. Towards a carbon independent and CO2-free electrochemical membrane process for NH3 synthesis. *Physical Chemistry Chemical Physics*, 16 (13):6129–6138, 2014. ISSN 14639076. doi: 10.1039/c4cp00173g.

[41] David J. Lampert, Hao Cai, and Amgad Elgowainy. Wells to wheels: Water consumption for transportation fuels in the United States. *Energy and Environmental Science*, 9(3):787–802, 2016. ISSN 17545706. doi: 10.1039/c5ee03254g.

[42] Rong Lan and Shanwen Tao. Electrochemical synthesis of ammonia directly from air and water using a Li+/H+/NH4+ mixed conducting electrolyte. *RSC Advances*, 3(39):18016–18021, 10 2013. ISSN 20462069. doi: 10.1039/c3ra43432j. URL www.rsc.org/advances.

[43] Rong Lan, John T.S. Irvine, and Shanwen Tao. Ammonia and related chemicals as potential indirect hydrogen storage materials. *International Journal of Hydrogen Energy*, 37(2):1482–1494, 2012. ISSN 03603199. doi: 10.1016/j.ijhydene.2011.10.004.

[44] Yongjun Leng, Guang Chen, Alfonso J Mendoza, Timothy B Tighe, Michael A Hickner, and Chao-Yang Wang. Solid-State Water Electrolysis with an Alkaline Membrane. *J. Am. Chem. Soc*, 134:9054–9057, 2012. doi: 10.1021/ja302439z. URL https://pubs.acs.org/sharingguidelines.

[45] Zhi Jie Li, Rui Quan Liu, Ji De Wang, Ya Hong Xie, and Fan Yue. Preparation of BaCe0.8Gd0.2O3-δ by the citrate method and its application in the synthesis of ammonia at atmospheric pressure. *Journal of Solid State Electrochemistry*, 9(4):201–204, 2005. ISSN 14328488. doi: 10.1007/s10008-004-0582-1.

[46] Linde CryoPlants Ltd. GAN containerized supply solutions for gaseous and liquid nitrogen. Technical report, 2019. URL https://www.linde-engineering.com/en/process-plants/air-separation-plants/containerised-air-separation-plants/index.html#:~:text=Itsupportsproductionratesof,upto99.9995%25asstandard.&text=Liquidnitrogencanbestored,providestrategicreservesof.

[47] Rui Quan Liu, Ya Hong Xie, Ji De Wang, Zhi Jie Li, and Ben Hui Wang. Synthesis of ammonia at atmospheric pressure with Ce0.8M 0.2O2-δ (M = La, Y, Gd, Sm) and their proton conduction at intermediate temperature. *Solid State Ionics*, 177(1-2):73–76, 1 2006. ISSN 01672738. doi: 10.1016/j.ssi.2005.07.018.

[48] Ruiquan Liu and Gaochao Xu. Comparison of electrochemical synthesis of ammonia by using sulfonated polysulfone and nafion membrane with Sm1.5Sr0.5NiO4. *Chinese Journal of Chemistry*, 28(2):139–142, 2010. ISSN 1001604X. doi: 10.1002/cjoc.201090044.

[49] Douglas R. MacFarlane, Pavel V. Cherepanov, Jaecheol Choi, Bryan H.R. Suryanto, Rebecca Y. Hodgetts, Jacinta M. Bakker, Federico M. Ferrero Vallana, and Alexandr N. Simonov. A Roadmap to the Ammonia Economy. *Joule*, 4(6):1186–1205, 2020. ISSN 25424351. doi: 10.1016/j.joule.2020.04.004. URL https://doi.org/10.1016/j.joule.2020.04.004.

[50] Mahdi Malmali, Yongming Wei, Alon Mccormick, and Edward L Cussler. Ammonia Synthesis at Reduced Pressure via Reactive Separation. *Ind. Eng. Chem. Res.*, 55:8922–8932, 2016. doi: 10.1021/acs.iecr.6b01880. URL https://pubs.acs.org/sharingguidelines.

[51] Mahdi Malmali, Giang Le, Jennifer Hendrickson, Joshua Prince, Alon V. McCormick, and E. L. Cussler. Better Absorbents for Ammonia Separation. *ACS Sustainable Chemistry and Engineering*, 6(5):6536–6546, 5 2018. ISSN 21680485. doi: 10.1021/acssuschemeng.7b04684. URL https://pubs.acs.org/sharingguidelines.

[52] Rami Mansouri, Ismail Boukholda, Mahmoud Bourouis, and Ahmed Bellagi. Modelling and testing the performance of a commercial ammonia/water absorption chiller using Aspen-Plus platform. *Energy*, 93(Part 2):2374–2383, 12 2015. ISSN 0360-5442. doi: 10.1016/J.ENERGY.2015.10.081.

[53] G. Marnellos, C. Athanasiou, P. Tsiakaras, and M. Stoukides. Modelling of solid oxide proton conducting reactor-cells: Thermodynamics and kinetics. *Ionics*, 2(5-6):412–420, 1996. ISSN 18620760. doi: 10.1007/BF02375820.

[54] George Marnellos and Michael Stoukides. Ammonia synthesis at atmospheric pressure. *Science*, 282(5386):98–100, 10 1998. ISSN 00368075. doi: 10.1126/science.282.5386.98. URL http://science.sciencemag.org/.

[55] Sandip Maurya, Sung Hee Shin, Yekyung Kim, and Seung Hyeon Moon. A review on recent developments of anion exchange membranes for fuel cells and redox flow batteries. *RSC Advances*, 5(47):37206–37230, 2015. ISSN 20462069. doi: 10.1039/c5ra04741b. URL http://dx.doi.org/10.1039/C5RA04741B.

[56] Konrad Meier. Hydrogen production with sea water electrolysis using Norwegian offshore wind energy potentials: Techno-economic assessment for an offshore-based hydrogen production approach with state-of-the-art technology. *International Journal of Energy and Environmental Engineering*, 5(2-3):1–12, 2014. ISSN 22516832. doi: 10.1007/s40095-014-0104-6.

[57] Eric R Morgan. Techno-Economic Feasibility Study of Ammonia Plants Powered by Offshore Wind. *University of Massachusetts - Amherst, PhD Dissertations*, page 432, 2013. URL http://scholarworks.umass.edu/open_access_dissertations/697.

[58] Teeranun Nakyai and Dang Saebea. Exergoeconomic comparison of syngas production from biomass, coal, and natural gas for dimethyl ether synthesis in single-step and two-step processes. *Journal of Cleaner Production*, 241:118334, 12 2019. ISSN 09596526. doi: 10.1016/j.jclepro.2019.118334.

[59] NASA. Carbon Dioxide | Vital Signs – Climate Change: Vital Signs of the Planet, 2020. URL https://climate.nasa.gov/vital-signs/carbon-dioxide/.

[60] Nel Hydrogen. Atmospheric Alkaline Electrolyser. URL https://nelhydrogen.com/product/atmospheric-alkaline-electrolyser-a-series/.

[61] The Truc Nguyen and Kazuyoshi Fushinobu. Effect of operating conditions and geometric structure on the gas crossover in PEM fuel cell. *Sustainable Energy Technologies and Assessments*, 37:100584, 2 2020. ISSN 22131388. doi: 10.1016/j.seta.2019.100584.

[62] Reza Omrani and Bahman Shabani. An analytical model for hydrogen and nitrogen crossover rates in proton exchange membrane fuel cells. *International Journal of Hydrogen Energy*, 45(55):31041–31055, 11 2020. ISSN 03603199. doi: 10.1016/j.ijhydene.2020.08.089.

[63] Ola Osman, Sgouris Sgouridis, and Andrei Sleptchenko. Scaling the production of renewable ammonia: A techno-economic optimization applied in regions with high insolation. *Journal of Cleaner Production*, 271, 10 2020. ISSN 09596526. doi: 10.1016/j.jclepro.2020.121627.

[64] Ola Osman, Sgouris Sgouridis, and Andrei Sleptchenko. Scaling the production of renewable ammonia: A techno-economic optimization applied in regions with high insolation. *Journal of Cleaner Production*, 271:121627, 10 2020. ISSN 09596526. doi: 10.1016/j.jclepro.2020.121627.

[65] H.G. Oswin and M. Salomon. THE ANODIC OXIDATION OF AMMONIA AT PLATINUM BLACK ELECTRODES IN AQUEOUS KOH ELECTROLYTE. *Canadian Journal of Chemistry*, 41:1686–1694, 2 1963.

[66] Hans Pasman. Industrial Processing Systems, Their Products and Hazards. *Risk Analysis and Control for Industrial Processes - Gas, Oil and Chemicals*, pages 1–31, 1 2015. doi: 10.1016/B978-0-12-800057-1.00001-8.

[67] Md Mamoon Rashid, Mohammed K Al Mesfer, Hamid Naseem, and Mohd Danish. Hydrogen Production by Water Electrolysis: A Review of Alkaline Water Electrolysis, PEM Water Electrolysis and High Temperature Water Electrolysis. *International Journal of Engineering and Advanced Technology*, 4(3):2249–8958, 2015.

[68] K H R Rouwenhorst, P M Krzywda, N E Benes, G Mul, and L Lefferts. *Chapter 4 - Ammonia Production Technologies*. Elsevier Inc., 2021. ISBN 9780128205600. doi: 10.1016/B978-0-12-820560-0.00004-7. URL http://dx.doi.org/10.1016/B978-0-12-820560-0.00004-7.

[69] D. M. Ruthven, N. S. Raghavan, and M. M. Hassan. Adsorption and diffusion of nitrogen and oxygen in a carbon molecular sieve. *Chemical Engineering Science*, 41(5):1325–1332, 1986. ISSN 00092509. doi: 10.1016/0009-2509(86)87105-6.

[70] Jafar Sadeghzadeh Ahari, Saeed Pakseresht, Mohammad Mahdyarfar, Saeed Shokri, Yahya Zamani, Ali Nakhaei Pour, and Fahimeh Naderi. Predictive dynamic model of air separation by pressure swing adsorption. *Chemical Engineering and Technology*, 29(1):50–58, 2006. ISSN 09307516. doi: 10.1002/ceat.200500226.

[71] Jafar Sadeghzadeh Ahari, Saeed Pakseresht, Mohammad Mahdyarfar, Saeed Shokri, Yahya Zamani, Ali Nakhaei Pour, and Fahimeh Naderi. Predictive dynamic model of air separation by pressure swing adsorption. *Chemical Engineering and Technology*, 29(1):50–58, 2006. ISSN 09307516. doi: 10.1002/ceat.200500226.

[72] Antonio Sánchez and Mariano Martín. Scale up and scale down issues of renewable ammonia plants: Towards modular design. *Sustainable Production and Consumption*, 16:176–192, 2018. ISSN 23525509. doi: 10.1016/j.spc.2018.08.001.

[73] J. Schramm, J. N. Klüssmann, L. R. Ekknud, and A. Ivarsson. Ammonia Application in IC Engines. *Advanced Motor Fuels Technology Collaboration Programme*, 2020.

[74] Siemens AG. Hydrogen Solutions | Renewable Energy. URL https://new.siemens.com/in/en/products/energy/renewable-energy/hydrogen-solutions.html.

[75] Felice Simonelli, Wijnand Stoefs, Jacopo Timini, Lorenzo Colantoni, Vasileios Rizos, Infelise Federico, and Giacomo Luchetta. For a Study on Composition and Drivers of Energy Prices and Costs in Energy Intensive Industries: the Case of the Chemical Industry-Ammonia. Technical Report January, Centre for European Policy Studies, 2014.

[76] A. R. Smith and J. Klosek. A review of air separation technologies and their integration with energy conversion processes. *Fuel Processing Technology*, 70(2):115–134, 5 2001. ISSN 03783820. doi: 10.1016/S0378-3820(01)00131-X.

[77] Collin Smith, Alon V. McCormick, and E. L. Cussler. Optimizing the Conditions for Ammonia Production Using Absorption. *ACS Sustainable Chemistry and Engineering*, 7(4):4019–4029, 2 2019. ISSN 21680485. doi: 10.1021/acssuschemeng.8b05395. URL https://pubs.acs.org/sharingguidelines.

[78] Collin Smith, Alfred K. Hill, and Laura Torrente-Murciano. Current and future role of Haber-Bosch ammonia in a carbon-free energy landscape. *Energy and Environmental Science*, 13(2):331–344, 2020. ISSN 17545706. doi: 10.1039/c9ee02873k.

[79] Thomas Sperle, De Chen, Rune Lødeng, and Anders Holmen. Pre-reforming of natural gas on a Ni catalyst. Criteria for carbon free operation. *Applied Catalysis A: General*, 282(1-2):195–204, 3 2005. ISSN 0926860X. doi: 10.1016/j.apcata.2004.12.011.

[80] Svetlana Ivanova and Robert Lewis. Producing Nitrogen via Pressure Swing Adsorption. Technical report, American Institute of Chemical Engineers - Air Products, 2012.

[81] P. Temluxame, P. Puengjinda, S. Peng-ont, W. Ngampuengpis, N. Sirimungkalakul, T. Jiwanuruk, T. Sornchamni, and P. Kim-Lohsoontorn. Comparison of ceria and zirconia based electrolytes for solid oxide electrolysis cells. *International Journal of Hydrogen Energy*, 4 2020. ISSN 03603199. doi: 10.1016/j.ijhydene.2020.03.121.

[82] Trevor Brown. Ammonia production causes 1% of total global GHG emissions, 4 2016. URL https://ammoniaindustry.com/ammonia-production-causes-1-percent-of-total-global-ghg-emissions/.

[83] United Nations. Paris Agreement. Technical report, 2015.

[84] United States Environmental Protection Agency. Overview of Greenhouse Gases | Greenhouse Gas (GHG) Emissions, 2018. URL https://www.epa.gov/ghgemissions/overview-greenhouse-gases#carbon-dioxide.

[85] Inc Universal Industrial Gases. Composition of Air - Components & Properties of Air, 2003. URL http://www.uigi.com/air.html.

[86] US Department of Commerce - NOAA - Global Monitoring Laboratory. Global Monitoring Laboratory - Carbon Cycle Greenhouse Gases, 2021.

[87] U.S. Global Change Research Program. Climate science special report: Fourth national climate assessment, volume I. *U.S. Global Change Research Program*, 1:470, 2018. ISSN 0736-6825. doi: 10.7930/J0J964J6. URL https://science2017.globalchange.gov/downloads/CSSR2017_FullReport.pdf%0Ascience2017.globalchange.gov.

[88] Cornelis J.M. Van Der Ham, Marc T.M. Koper, and Dennis G.H. Hetterscheid. Challenges in reduction of dinitrogen by proton and electron transfer. *Chemical Society Reviews*, 43(15):5183–5191, 2014. ISSN 14604744. doi: 10.1039/c4cs00085d.

[89] Jadran Vrabec, Gaurav Kumar Kedia, Ulrich Buchhauser, Roland Meyer-Pittroff, and Hans Hasse. Thermodynamic models for vapor-liquid equilibria of nitrogen + oxygen + carbon dioxide at low temperatures. *Cryogenics*, 49(2):72–79, 2 2009. ISSN 00112275. doi: 10.1016/j.cryogenics.2008.11.002.

[90] Lu Wang, Meikun Xia, Hong Wang, Kefeng Huang, Chenxi Qian, Christos T. Maravelias, and Geoffrey A. Ozin. Greening Ammonia toward the Solar Ammonia Refinery. *Joule*, 2(6):1055–1074, 2018. ISSN 25424351. doi: 10.1016/j.joule.2018.04.017. URL https://doi.org/10.1016/j.joule.2018.04.017.

[91] Miao Wang, Mohd A. Khan, Imtinan Mohsin, Joshua Wicks, Alexander H. Ip, Kazi Z. Sumon, Cao-Thang Dinh, Edward H. Sargent, Ian D. Gates, and Md Golam Kibria. Can sustainable ammonia synthesis pathways compete with fossil-fuel based Haber–Bosch processes? (ESI). *Energy & Environmental Science*, 14(5):2535–2548, 2021. ISSN 1754-5692. doi: 10.1039/d0ee03808c.

[92] Miao Wang, Mohd A. Khan, Imtinan Mohsin, Joshua Wicks, Alexander H. Ip, Kazi Z. Sumon, Cao-Thang Dinh, Edward H. Sargent, Ian D. Gates, and Md Golam Kibria. Can sustainable ammonia synthesis pathways compete with fossil-fuel based Haber–Bosch processes? *Energy & Environmental Science*, 14(5):2535–2548, 2021. ISSN 1754-5692. doi: 10.1039/d0ee03808c.

[93] W. B. Wang, X. B. Cao, W. J. Gao, F. Zhang, H. T. Wang, and G. L. Ma. Ammonia synthesis at atmospheric pressure using a reactor with thin solid electrolyte BaCe0.85Y0.15O3-α membrane. *Journal of Membrane Science*, 360(1-2):397–403, 2010. ISSN 03767388. doi: 10.1016/j.memsci.2010.05.038.

[94] Qiushi Wei, Jolie M. Lucero, James M. Crawford, J. Douglas Way, Colin A. Wolden, and Moises A. Carreon. Ammonia separation from N2 and H2 over LTA zeolitic imidazolate framework membranes. *Journal of Membrane Science*, 623:119078, 4 2021. ISSN 18733123. doi: 10.1016/j.memsci.2021.119078.

[95] Lien-Chun Weng, Alexis T. Bell, and Adam Z. Weber. Towards membrane-electrode assembly systems for CO2 reduction: a modeling study. *Energy & Environmental Science*, 12(6):1950–1968, 6 2019. ISSN 1754-5706. doi: 10.1039/C9EE00909D. URL https://pubs-rsc-org.tudelft.idm.oclc.org/en/content/articlehtml/2019/ee/c9ee00909dhttps://pubs-rsc-org.tudelft.idm.oclc.org/en/content/articlelanding/2019/ee/c9ee00909d.

[96] Xing L. Yan and Ryutaro Hino. *Nuclear Hydrogen Production Handbook*. CRC Press, 2011. URL https://books.google.nl/books?hl=nl&lr=&id=FUf-fjlK_CEC&oi=fnd&pg=PR2&ots=3BcoV8vi6U&sig=V8tbAuJsX33GNknb-GZjZV4X6zs&redir_esc=y#v=onepage&q&f=false.

[97] Gaochao Xu, Ruiquan Liu, and Jin Wang. Electrochemical synthesis of ammonia using a cell with a Nafion membrane and SmFe0.7Cu0.3-x Ni x O3 (x = 0-0.3) cathode at atmospheric pressure and lower temperature. *Science in China, Series B: Chemistry*, 52(8):1171–1175, 2009. ISSN 10069291. doi: 10.1007/s11426-009-0135-7.

[98] Seong Bin Yu, Seung Ho Lee, Muhammad Taqi Mehran, Jong Eun Hong, Jong Won Lee, Seung Bok Lee, Seok Joo Park, Rak Hyun Song, Joon Hyung Shim, Yong Gun Shul, and Tak Hyoung Lim. Syngas production in high performing tubular solid oxide cells by using high-temperature H2O/CO2 co-electrolysis. *Chemical Engineering Journal*, 335:41–51, 3 2018. ISSN 13858947. doi: 10.1016/j.cej.2017.10.110.

[99] Yanjie Zheng, Rodrigo Caceres Gonzalez, Marta C. Hatzell, and Kelsey B. Hatzell. Concentrating solar thermal desalination: Performance limitation analysis and possible pathways for improvement. *Applied Thermal Engineering*, 184:116292, 2 2021. ISSN 13594311. doi: 10.1016/j.applthermaleng.2020.116292.